



UNIVERSITY OF CRETE
DEPARTMENT OF MATERIALS SCIENCE & TECHNOLOGY

BACHELOR THESIS

Promotion of the osteogenic differentiation of pre-osteoblastic cells
in piezoelectric porous scaffolds under mechanical stimulation

NIKOLETA NATALIA TAVERNARAKI

SUPERVISOR: Maria Chatzinikolaidou, Associate Professor

CO-SUPERVISOR: Maria Vamvakaki, Professor

HERAKLION OCTOBER 2023



ΠΑΝΕΠΙΣΤΗΜΙΟ ΚΡΗΤΗΣ
ΤΜΗΜΑ ΕΠΙΣΤΗΜΗΣ ΚΑΙ ΤΕΧΝΟΛΟΓΙΑΣ ΥΛΙΚΩΝ

ΠΤΥΧΙΑΚΗ ΕΡΓΑΣΙΑ

Αύξηση της οστεογενούς διαφοροποίησης προ-οστεοβλαστών σε
πιεζοηλεκτρικά πορώδη ικρίσματα με χρήση μηχανικής διέγερσης

ΝΙΚΟΛΕΤΑ ΝΑΤΑΛΙΑ ΤΑΒΕΡΝΑΡΑΚΗ

ΕΠΙΒΛΕΠΟΥΣΑ: Μαρία Χατζηνικολαΐδου, αναπληρώτρια καθηγήτρια

ΣΥΝΕΠΙΒΛΕΠΟΥΣΑ: Μαρία Βαμβακάκη, καθηγήτρια

ΗΡΑΚΛΕΙΟ ΟΚΤΩΒΡΙΟΣ 2023

Δήλωση Συγγραφικής Ιδιότητας

Εγώ, η Νικολέτα Ναταλία Ταβερναράκη, δηλώνω ότι αυτή η πτυχιακή εργασία με τίτλο, «*Promotion of the osteogenic differentiation of pre-osteoblastic cells in piezoelectric porous scaffolds under mechanical stimulation / Αύξηση της οστεογενούς διαφοροποίησης προ-οστεοβλαστών σε πιεζοηλεκτρικά πορώδη ικριώματα με χρήση μηχανικής διέγερσης*», και η δουλειά που παρουσιάζεται σε αυτή είναι δική μου, και μέρος εκείνης έγινε σε συνεργασία με την υποψήφια διδάκτορα κ. Πλατανιά Βαρβάρα. Επιβεβαιώνω ότι:

- Αυτή η δουλειά πραγματοποιήθηκε ολοκληρωτικά ή κυρίως κατά την υποψηφιότητά μου για τον τίτλο προπτυχιακών σπουδών σε αυτό το πανεπιστήμιο.
- Όπου οποιοδήποτε μέρος αυτής της πτυχιακής εργασίας έχει προηγουμένως κατατεθεί για την απόκτηση πτυχίου ή άλλου τίτλου σε αυτό ή άλλο πανεπιστήμιο, αυτό διατυπώνεται ξεκάθαρα.
- Όπου έχω συμβουλευτεί την δημοσιευμένη δουλειά τρίτων, αυτό αποδίδεται ορθώς.
- Όπου έχω παραθέσει από δουλειά τρίτων, η πηγή δίνεται πάντα. Με εξαίρεση αυτές τις παραθέσεις, αυτή η πτυχιακή εργασία είναι εξ ολοκλήρου προσωπική μου δουλειά.
- Έχω παραθέσει όλες τις κύριες πηγες βοήθειας.
- Όπου αυτή η πτυχιακή εργασία είναι βασισμένη σε συνεργατική δουλειά δική μου και τρίτων, έχω καταστήσει ξεκάθαρο ποια κομμάτια έχουν πραγματοποιηθεί από άλλους και πως συνέβαλα εγώ.

Ημερομηνία:

Υπογραφή:

Contents

Acknowledgements	6
Abstract	7
Περίληψη	8
Chapter 1. Introduction.....	9
Chapter 2. Materials and methods	11
2.1. Preparation of porous scaffolds comprising poly(vinyl alcohol), gelatin and a piezoelectric polymer, poly(3,4-ethylenedioxythiophene) (PEDOT:PSS)	11
2.2. Physicochemical and mechanical characterization of the scaffolds	12
2.2.1. Fourier transform infrared spectroscopy (FTIR).....	12
2.2.2. Determination of the degradation rate.....	12
2.2.3. Liquid uptake measurement	12
2.2.4. Pore size and porosity quantification.....	13
2.2.5. Electrical conductivity	13
2.2.6. Mechanical characterization of the scaffolds	13
2.3. Evaluation of cytotoxicity and cell adhesion of cell-laden scaffolds.....	14
2.3.1. Cell culture maintenance	14
2.3.2. Cell viability evaluation by metabolic assay PrestoBlue™	14
2.3.3. Cell adhesion and morphology.....	14
2.4. Osteogenic response of MC3T3-E1 pre-osteoblastic cells under mechanical stimulation	14
2.4.1. Cell seeding of scaffolds prior mechanical stimulation	14
2.4.2. Mechanical stimulation protocol	15
2.4.3. Cell viability of cell-laden scaffolds (constructs) via Live/Dead assay.....	15
2.4.4. Determination of alkaline phosphatase (ALP) activity	16
2.4.5. Calcium secretion measurements	16
2.4.6. Quantification of secreted collagen by cells within the constructs	16
2.4.7. Energy dispersive spectroscopy (EDS) analysis	16
2.4.8. X-ray diffraction (XRD) analysis	17
2.5. Statistical analysis.....	17
Chapter 3. Results	18
3.1. Physicochemical and mechanical characterization of scaffolds.....	18
3.1.1. Scaffolds' morphology at macroscopic and microscopic view	18
3.1.2. FTIR spectra analysis.....	18
3.1.3. Degradation analysis	19
3.1.4. Swelling ratios	20
3.1.5. Porosity of scaffolds	21

3.1.6. Electrical conductivity	22
3.1.7. Evaluation of the scaffolds' mechanical properties	22
3.2. Evaluation of cell adhesion, morphology, viability and proliferation within scaffolds	23
3.2.1. Viability and proliferation of pre-osteoblastic cells within the scaffolds.....	23
3.2.2. Cell adhesion and morphology of pre-osteoblastic cells within the scaffolds.....	24
3.3. Osteogenic response of MC3T3-E1 pre-osteoblastic cells on the piezoelectric scaffolds under mechanical stimulation	24
3.3.1. Morphology of pre-osteoblastic cells within the constructs.....	24
3.3.2. Live/Dead assay.....	25
3.3.3. Determination of the alkaline phosphatase activity	26
3.3.4. Calcium secretion measurement.....	27
3.3.5. Collagen secretion quantification.....	28
3.3.6. Energy dispersive spectroscopy (EDS) analysis of biomineralization.....	28
3.3.7. X-ray diffraction (XRD) analysis of biomineralization.....	30
Chapter 4. Discussion	31
Chapter 5. Conclusion	36
References.....	37

Acknowledgements

I would like to express my sincere gratitude to my esteemed Professor, Maria Chatzinikolaïdou, for her invaluable guidance, expertise, and unwavering support throughout my bachelor thesis journey. I am truly grateful to have had the opportunity to learn from such a dedicated and inspiring person, who has placed their trust in me far more than I ever did in myself, and who has provided me with incredible opportunities to work on remarkable and challenging projects. Her expertise and mentorship have been invaluable, and I am truly thankful for the opportunity she provided me to explore and contribute to my chosen field of study.

I wish to express my profound gratitude to my co-advisor, Professor Maria Vamvakaki, for her support and guidance throughout my academic journey. Her exceptional teaching during my undergraduate studies laid the essential foundation for my understanding of soft matter chemistry, which constitutes a significance component of my thesis. It has been an honor to have you as mentor.

I would like to extend my heartfelt gratitude to my beloved colleague and friend, Varvara. Throughout our journey together in the lab, Varvara has been a source of inspiration and support. Her passion for science and her boundless enthusiasm have not only made our work pleasant but have also inspired me. I am deeply thankful for her endless patience with me and the countless moments of guidance, encouragement and friendship that Varvara has shared with me. I am really grateful and privileged to have had her by my side.

To all lab members, I want to express my appreciation for their continuous assistance whenever I needed it, and for creating a pleasant atmosphere in the lab. Your contributions have made a significant impact on my growth, and I am truly fortunate to have you by my side.

To my parents, Nektarios and Eleni, I am deeply grateful, who always pushed me to pursue my dreams and aspirations and guided me through life with boundless love and care. Your confidence in me and your presence throughout my journey has been a source of motivation and inspiration. Also, I want to thank my little sister, Eirini, for always supporting me and bringing a smile to my face even during my most challenging moments.

Finally, to my dear friends, I cannot thank you enough for your relentless encouragement, understanding, and love. Thank you for believing in me and for being there every step of the way.

Abstract

Bone is a highly dynamic tissue that undergoes continuous mechanical forces throughout life. Mechanical stimuli applied on scaffolds resembling a part of the human bone tissue could have major effect on osteogenesis. However, the precise conditions governing this process remain largely unexplored. Poly(3,4-ethylenedioxythiophene) polystyrene sulfonate (PEDOT:PSS) is a piezoelectric material that responds to mechanical stimulation, producing an electrical signal that promotes the osteogenic differentiation of pre-osteoblastic cells by opening voltage-gated calcium channels. The aim of this study was to examine the biological behavior of mouse calvaria osteoblastic precursor cells (MC3T3-E1) when seeded onto lyophilized piezoelectric PEDOT:PSS-containing scaffolds applying uniaxial compression. Two different concentrations of PEDOT:PSS (0.15% w/v and 0.10% w/v) were combined with a 5% w/v poly(vinyl alcohol) (PVA) and 5% w/v gelatin, casted into wells, freeze dried and crosslinked with 2% v/v (3-glycidyloxypropyl)trimethoxysilane (GOPS) and 0.025% w/v glutaraldehyde. The scaffolds were physicochemically characterized by Fourier transform infrared spectroscopy (FTIR), measurement of elastic modulus, swelling ratio, degradation rate. Scaffolds seeded with pre-osteoblastic cells were subjected to uniaxial compression with a frequency of 1 Hz and a strain of 10% for 1 h daily for 21 days, and their osteogenic response was compared to that of a non-mechanically stimulated culture, the static one. The loading parameters were selected to resemble the *in vivo* loading situation. Cell viability and morphology of the MC3T3-E1 pre-osteoblasts seeded on the PEDOT:PSS/PVA/gelatin scaffolds were determined. The alkaline phosphatase (ALP) activity, the collagen and calcium production were assessed to validate the effect of the piezoelectric scaffolds in presence (dynamic culture) and in absence (static culture) of the mechanical stimuli towards the osteogenic differentiation process of the pre-osteoblasts. PEDOT:PSS/PVA/gelatin scaffolds presented favorable mechanical properties for bone tissue engineering. Their elastic modulus ranged between 1 and 5 MPa. The degradation rates indicate a mass loss up to 15% after 21 days. The cell viability indicates an increase of cell number over time, while scanning electron microscopy (SEM) images display well-spread cells morphology. The ALP activity at days 3 and 7 is higher in the dynamic culture compared to the static one. Increased ALP activity and profound collagen and calcium secretion further validate osteogenic response. Moreover, energy dispersive spectroscopy (EDS) analysis revealed the presence of calcium phosphate in the extracellular matrix after 21 days. Our results indicate that the PEDOT:PSS/PVA/gelatin scaffolds support the adhesion, proliferation, and osteogenic differentiation of the pre-osteoblastic cells under mechanical stimulation, thus favoring bone and other load-bearing tissue engineering with amplified matrix production. Furthermore, the development of a comprehensive 3D mechano-active model, establishes an innovative platform for studying osteogenesis under conditions closely resembling the body natural state. This approach not only contributes to advancing *in vitro* evaluation methods but also significantly reduces the need for *in vivo* experimentation.

Keywords: Dynamic vs. static culture, gelatin, mechanical stimulation, PEDOT:PSS scaffolds, piezoelectric material, poly(vinyl alcohol)

Περίληψη

Το οστό είναι ένας δυναμικός ιστός που υφίσταται συνεχείς πιέσεις κατά τη διάρκεια της ζωής του ανθρώπου. Τρισδιάστατα (3Δ) ικριώματα που επιδέχονται μηχανικές πιέσεις επάγοντας την οστεογένεση θα μπορούσαν να συμβάλουν σημαντικά στη μηχανική του οστίτη ιστού για την αναγέννησή του. Το πολυ(3,4-αιθυλενδιοξυθειοφένιο) σουλφονικό πολυστυρένιο (PEDOT:PSS) είναι ένα πιεζοηλεκτρικό υλικό που ανταποκρίνεται σε μηχανικά ερεθίσματα παράγοντας ένα ηλεκτρικό σήμα που επάγει την οστεογένεση ανοίγοντας τις τασσεοελεγχόμενες αντλίες ασβεστίου στις κυτταρικές μεμβράνες. Στην παρούσα μελέτη εξετάζουμε τη βιολογική συμπεριφορά προ-οστεοβλαστικών κυττάρων MC3T3-E1 πάνω σε ικριώματα που περιέχουν PEDOT:PSS, μετά από εφαρμογή μηχανικής διέγερσης. Δύο συγκεντρώσεις PEDOT:PSS (0.15% w/v και 0.10% w/v) ομογενοποιήθηκαν με υδατικό αιώρημα 5% w/v πολυβινυλικής αλκοόλης (PVA) και 5% w/v ζελατίνης (gel), και διασταυρώθηκαν μέσω 2%v/v (3-γλυκιδυλοξυ)προπυλο-τριμεθοξυ-σιλανίου και 0.025% v/v γλουταραλδεΐδης. Εξετάστηκαν οι φυσικοχημικές ιδιότητες των δειγμάτων όπως η ελαστικότητα και ο ρυθμός αποδόμησης. Ικριώματα στα οποία εναποτέθηκαν προ-οστεοβλαστικά κύτταρα, υποβλήθηκαν σε μηχανική διέγερση μιας ώρας με συχνότητα 1 Hz και παραμόρφωση 10% για 21 ημέρες και τα αποτελέσματα συγκρίθηκαν με αυτά μιας παράλληλης στατικής καλλιέργειας. Οι παράμετροι επιλέχθηκαν με κριτήριο την φυσιολογική κατάσταση του οργανισμού. Μελετήθηκε η βιωσιμότητα, ο πολλαπλασιασμός και η μορφολογία των κυττάρων. Επιπλέον εξετάστηκε η διαφοροποιητική δυναμική των προ-οστεοβλαστών. Τα πρώτα στάδια της οστεογένεσης αξιολογήθηκαν μέσω της δραστηριότητας της αλκαλικής φωσφατάσης. Επίσης, έγινε ποσοτικοποίηση του εκκρινόμενου από τα κύτταρα κολλαγόνου και ασβεστίου, δείκτες που σηματοδοτούν τον σχηματισμό εξωκυττάριας μήτρας του οστού. Το μέτρο ελαστικότητας των ικριωμάτων κυμάνθηκε μεταξύ 1-5 MPa, ενώ ο ρυθμός αποδόμησης τους υπολογίστηκε σε 15% μετά από 21 ημέρες, ιδανικά χαρακτηριστικά για εφαρμογές στην μηχανική οστίτη ιστού. Παρατηρήθηκε καλή κυτταρική προσκόλληση και αύξηση του κυτταρικού πολλαπλασιασμού με την πάροδο του χρόνου. Η δραστηριότητα της αλκαλικής φωσφατάσης ήταν σημαντικά υψηλότερη στα ικριώματα που υποβλήθηκαν σε μηχανική διέγερση (δυναμική καλλιέργεια), σε σύγκριση με την στατική καλλιέργεια. Επιπλέον, στην δυναμική καλλιέργεια παρατηρήθηκε ενασβεστωση με σχηματισμό υδροξυαπατίτη μετά από 21 μέρες. Η παραπάνω μελέτη υποδεικνύει ότι η ανάπτυξη μηχανικά ευαίσθητων ικριωμάτων συμβάλλει σημαντικά στην αναγέννηση οστίτη ιστού. Τα ικριώματα που αναπτύξαμε από PEDOT:PSS/PVA/gel υποστηρίζουν την προσκόλληση, τον πολλαπλασιασμό και την οστεογενή διαφοροποίηση των προ-οστεοβλαστών υπό μηχανική διέγερση, προσομοιάζοντας την φυσιολογική δυναμική κατάσταση των οστών. Τα παραπάνω αποτελέσματα καθιστούν τα συγκεκριμένα ικριώματα υποσχόμενα για εφαρμογές στη μηχανική οστίτη ιστού ή άλλων τύπων ιστών με πιεζοηλεκτρικές ιδιότητες. Επίσης, η ανάπτυξη ενός ολιστικού μοντέλου 3Δ τασσεοελεγχόμενων ικριωμάτων με προ-οστεοβλάστες σε δυναμική καλλιέργεια αποτελεί ένα πρωτοποριακό σύστημα μελέτης και αξιολόγησης της οστεογένεσης σε δυναμικές συνθήκες παρόμοιες με τις φυσιολογικές του οργανισμού. Αυτή η δυνατότητα συμβάλλει στην εξέλιξη καινοτόμων in vitro μεθόδων αξιολόγησης με το σημαντικό πλεονέκτημα της μείωσης των in vivo πειραμάτων.

Λέξεις κλειδιά: Δυναμική και στατική καλλιέργεια, μηχανική διέγερση, ζελατίνη, PEDOT:PSS ικριώματα, πιεζοηλεκτρικό υλικό, PVA

Chapter 1. Introduction

Bone disorders pose significant concerns due to the rising median age within our population. There is a high prevalence of large-scale bone defects, such as non-healing fractures, bone tumors, and craniofacial surgery, which inflict substantial physical and psychological discomfort on patients. Extensive research efforts have focused on regenerating existing bone or replacing lost bone using complex biomaterials and tissue engineering techniques [1, 2]. Initially, these biomaterials were selected based on their biomechanical properties for structural restoration [3, 4]. Later, bioactive and bioresorbable scaffolds were engineered to promote tissue growth [5, 6]. Presently, innovative scaffolds are being designed to induce bone formation and vascularization [7-9]. However, achieving optimal tissue growth and regeneration remains a considerable obstacle. In recent years, the use of stimuli-responsive biomaterials in bone tissue engineering has emerged as a promising approach to address these challenges. These biomaterials can trigger specific responses through external stimuli, such as mechanical forces, leading to enhanced tissue regeneration [10, 11]. Piezoelectric materials have gained attention for their potential in generating electrical signals in response to mechanical stimulation, thereby promoting osteogenic differentiation [12, 13].

Bone tissue is characterized by its dynamic nature and constant exposure to mechanical forces throughout life, exhibiting high responsiveness to such stimuli [14]. Scaffolds have played a vital role in major advancements in bone tissue engineering. Conductive materials have shown potential in supporting osteogenesis *in vitro* and bone regeneration *in vivo* [15]. In this context, scaffolds incorporating poly(3,4-ethylenedioxythiophene) polystyrene sulfonate (PEDOT:PSS) serve as intriguing substrates for promoting osteogenic differentiation [16]. PEDOT:PSS, a piezoelectric material, possesses the unique property of generating electrical signals in response to mechanical stimulation [17]. This electrical signal has been shown to facilitate the opening of voltage-gated calcium channels, thereby playing a crucial role in promoting the osteogenic differentiation of pre-osteoblastic cells. Moreover, it has been found that the presence of PEDOT:PSS could potentially enhance the mechanical properties of the scaffold making it more adequate for bone tissue engineering applications [18, 19].

Gelatin is a natural polymer derived from collagen and major component of the extracellular matrix (ECM) in bone tissue standing out for its biocompatibility. Its inherent ability to mimic the biochemical and mechanical cues of native bone facilitates enhanced cell-scaffold interactions ensuring minimal immune response after implantation. Moreover, gelatin exhibits excellent biodegradability, allowing for gradual scaffold degradation, coinciding with new tissue formation [20-22]. Poly(vinyl alcohol) (PVA) is a synthetic polymer widely known for its excellent biocompatibility, hydrophilicity, and biodegradability, making it an ideal candidate for bone tissue engineering applications. PVA scaffolds can be tailored to possess tunable mechanical properties and porosity, enabling the provision of adequate mechanical support and nutrient transport for cell growth and tissue development. Furthermore, PVA has been shown to enhance cellular attachment and proliferation, facilitating a conducive environment for osteogenic differentiation and mineralization, which are crucial for the formation of functional bone tissue [23]. Combining gelatin and PVA into polymeric matrices provides a synergistic effect, incorporating the advantages of both polymers. These matrices offer enhanced mechanical strength, improved biocompatibility, and a biomimetic environment for bone regeneration. The gelatin-PVA co-polymer matrices provide a favorable platform for cell attachment, proliferation, and osteogenic differentiation [24]. The incorporation of PEDOT:PSS was motivated by its ability to convert mechanical stimuli into electrical signals [25], which have been shown to activate voltage-gated calcium channels of the cell membrane [26], a known regulator of osteogenic differentiation [27]. By combining these three components, we aimed to create multifunctional scaffolds that not only provide structural support and biocompatibility through PVA and gelatin but also harnesses the piezoelectric properties of PEDOT:PSS to potentially enhance osteogenic differentiation under mechanical stimulation.

By investigating the cellular responses of mouse calvaria osteoblastic precursor cell line (MC3T3-E1) cultured on lyophilized piezoelectric PEDOT:PSS/PVA/gelatin scaffolds under osteogenic

conditions and mechanical stimulation, we aimed to evaluate the suitability of these scaffolds for bone tissue engineering applications. The parameters were selected to resemble the *in vivo* loading situation [28]. Understanding the biological behavior and osteogenic potential of MC3T3-E1 on such scaffolds will provide insights into the capabilities of PEDOT:PSS-based scaffolds in promoting osteogenesis and contribute to the development of advanced strategies for bone tissue regeneration and repair.

Previous studies have demonstrated cell adhesion and viability on porous, freeze-dried PEDOT:PSS scaffolds using human mesenchymal stem cells or cardiomyoblasts [29]. However, a comprehensive examination of the effect of mechanically stimulated piezoelectric PEDOT:PSS-containing scaffolds to assess osteogenic differentiation remains limited. Our study seeks to fill this gap by focusing on the cell-biomaterial interactions and the osteoinductive potential of such three-dimensional (3D) scaffolds subjected to mechanical stimulation. Evidence of increased osteogenic differentiation potential is exhibited through the assessment of osteogenic markers such as alkaline phosphatase activity, collagen and calcium production, matrix mineralization, and hydroxyapatite (HA) formation. These findings underscore the versatility of PEDOT:PSS as a scaffold material for bone tissue engineering. By investigating the relationship between mechanical forces and osteogenic differentiation, our research aims to contribute to the expanding field of bone tissue engineering and lay the groundwork for innovative approaches in healthcare.

Chapter 2. Materials and methods

2.1. Preparation of porous scaffolds comprising poly(vinyl alcohol), gelatin and a piezoelectric polymer, poly(3,4-ethylenedioxythiophene) (PEDOT:PSS)

Two different scaffold compositions were prepared: (i) PEDOT:PSS/PVA/Gelatin and (ii) PVA/Gelatin as control. PEDOT:PSS-containing scaffolds were prepared from a stock 1.3% w/v PEDOT:PSS dispersion. The exact composition of the two polymers in the dispersion was 0.5% w/v PEDOT and 0.8% w/v PSS diluted in water. Two different concentrations of PEDOT:PSS were employed, 0.1% and 0.15% w/v, while keeping the PVA/Gelatin concentration constant at 5% w/v each. The concentration of 0.15% w/v was selected as it was the highest value that did not affect the biocompatibility of the scaffold. A lower concentration (0.1% w/v) was included in the study as a comparison to the 0.15% w/v composition, aiming to conclude the significance of PEDOT:PSS's integration to the final scaffolds based on their biological and mechanical attributes. PVA/Gelatin blends were prepared following an established protocol of our research group (unpublished data). For the solution, 0.15% w/v PEDOT:PSS, 20 ml deionized water was measured and poured into a vial with a magnet. Then the vial was autoclaved at 100 °C for 15 min to sterilize. Simultaneously, 1 gr of PVA was exposed to ultraviolet (UV) radiation for 15 min to sterilize and then added to the vial. The solution was kept under stirring for 3 h at 100 °C. After that, 1 g of gelatin was added to the mix, after being exposed to UV radiation for sterilization, as well. The solution was kept under stirring at 70 °C for another hour until the gelatin was completely dissolved. 2.4 ml PEDOT:PSS was then measured in the hood, and exposed to UV radiation for 15 min. While the PVA/gelatin solution was stirring, 2.4 ml of the solution was extracted and 2.4 ml PEDOT:PSS was added. The final solution was kept under stirring for 3 h at 70 °C. For the solution of 0.1% w/v PEDOT:PSS, the same procedure was followed with the respective concentration of PEDOT:PSS. For the control scaffold a solution of 5% w/v PVA and 5% w/v Gelatin was prepared without the addition of PEDOT:PSS. The final solutions were casted into each well of a 96 well-plate and four freezing/thawing cycles were provided [30] with the last cycle being the freezing. According to the literature, subjecting conductive polymers to repeated freeze-thaw cycles has the potential to reshape the polymer's microstructure, leading in a substantial enhancement of the mechanical and electrochemical properties of the final product [31]. The length of each cycle was 24 h. The freezing temperature was equal to -20 °C and the thawing temperature was equal to room temperature (RT). After four cycles hydrogels were freeze-dried for 45 min at -40 °C. By the time the freeze-drying process came to an end, the lyophilized samples were taken under the hood and half of each concentration was crosslinked. The crosslinker consisted of 2% v/v (3-glycidyloxypropyl) trimethoxysilane (GOPS) [17] and 0.025% v/v glutaraldehyde [32], each diluted in 10 ml phosphate buffer saline (PBS). After 15 min, the first crosslinker (GOPS) was extracted and the scaffolds were rinsed twice with PBS. Then the second crosslinker was added and after 15 min was extracted. The scaffolds were thoroughly rinsed with PBS in order to remove any unbound residues of crosslinker that might be cytotoxic during the biological evaluation. The fabrication protocol is displayed in Figure 1.

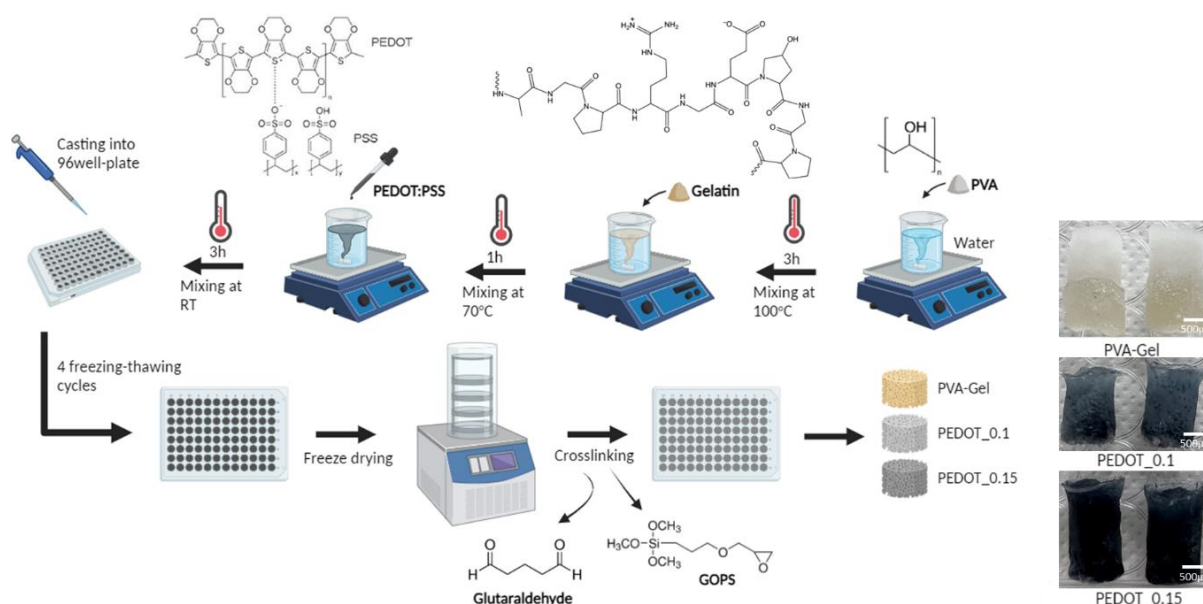


Figure 1. Schematic on the synthesis of scaffolds. The scale bar represents 500 μm .

2.2. Physicochemical and mechanical characterization of the scaffolds

2.2.1. Fourier transform infrared spectroscopy (FTIR)

FTIR analysis of the different blend scaffold compositions, as well as their basic components PEDOT:PSS, Gelatin and PVA in solid state was recorded in transmittance mode using a Nicolet 6700 optical spectrometer. For each spectrum, 32 scans were collected in the range of 4000-500 cm^{-1} . The spectral data were collected and the numerical values were transferred to GraphPad Prism 8 for graphical representation.

2.2.2. Determination of the degradation rate

Degradation rates determine the duration in which cells can substitute the artificial scaffold's synthetic extracellular matrix with their naturally generated matrix. *In vitro* degradation of the different scaffolds was assessed by immersing them in PBS and then letting them incubate at 37 $^{\circ}\text{C}$ and 5% CO_2 . Firstly, the scaffolds were weighed at day 0 and then allowed to incubate. The scaffolds were removed from the medium on day 4 and subsequently on days 7, 14, 21, and 28, slightly drained with a paper towel and their weight was measured by means of precision balance. Measurements were taken in seven replicates ($n=7$) of each scaffold type. The degradation rate was expressed as a percentage of weight loss in the biomaterial by the following formula:

$$\text{Degradation rate} : \frac{\text{weight}_{\text{day } 0} - \text{weight}_{\text{day } i}}{\text{weight}_{\text{day } 0}} \cdot 100\%$$

Where weight at day 0 is the initial weight of the scaffolds and weight at day i is the weight of the scaffolds at the respective days, starting with day 4.

2.2.3. Liquid uptake measurement

Water absorption is a critical attribute of materials, as it enables the uptake of nutrients from the immediate environment, vital for ensuring cell viability. Swelling of polymer materials is described as the process of penetration of solvent molecules into a polymer matrix causing a change in the volume [33]. The swelling capabilities of scaffolds were evaluated by letting them soak in the presence of PBS for approximately 15 min at RT. Then scaffolds were removed from the buffer, slightly drained with a

paper towel, and weighed by means of precision balance. Then the scaffolds were freeze-dried for 24 h to dry completely and weighed again. The liquid uptake ability was expressed as a percentage of weight increase in the biomaterial (n=7), by the following formula:

$$\text{Swelling ratio} : \frac{\text{weight}_{\text{wet}} - \text{weight}_{\text{dry}}}{\text{weight}_{\text{wet}}} \cdot 100\%$$

Where weight wet is the weight of the wet scaffolds and weight dry is the weight of the dry scaffolds.

2.2.4. Pore size and porosity quantification

The evaluation of % porosity was calculated via SEM images using ImageJ and through the liquid displacement method (Archimedes' principal). The liquid displacement method was conducted with water, which can penetrate the scaffold pores without any unwanted changes in size [34, 35]. The scaffolds were freeze-dried and then immersed in a pre-determined volume of water (V_1) The scaffolds remained in the solvent until no air bubbles emerged, indicating that the solvent had infuse the pores of the scaffold. The volume of the water and the solvent-saturated scaffolds was recorded as V_2 . Finally, the solvent-saturated scaffolds were removed and the residual volume of water was assessed (V_3). The porosity of the scaffolds was subsequently calculated using the following equation:

$$P \% = \frac{V_1 - V_3}{V_2 - V_3} \times 100\%$$

2.2.5. Electrical conductivity

The electrical conductivity was measured with the electromagnetic induction method, where the induction current generated by two coils immersed in the solution was evaluated. Electrical conductivity of PEDOT:PSS was measured using a Thermo Scientific™ Orion™ Versa Star Pro™ Conductivity Benchtop. Two different PEDOT:PSS-containing suspensions (0.1% w/v and 0.15% w/v PEDOT:PSS) were prepared alongside with the control composition of PVA/Gel, utilized as a comparative reference. The conductivity measurements were performed at room temperature. Prior to each measurement, the instrument was calibrated with double distilled water, a standard conductivity solution to guarantee accuracy. Seven different measurements were taken for each solution to ensure the reliability of the results (n=7). The collected data were transferred to GraphPad Prism 8 for graphical representation.

2.2.6. Mechanical characterization of the scaffolds

The effect of PEDOT:PSS incorporation into PVA/Gel on the hydrogels' mechanical properties was evaluated by uniaxial compression tests. The mechanical compression tests were performed by using a mechanical test system, (UniVert, CellScale, Waterloo, Canada) equipped with a 50 N sensor at RT. Cylindrical hydrogel samples with a diameter of 1 cm and approximately 2 cm high were employed. The measurements were performed in six replicates (n=6) from each scaffold composition and crosslinking method. Compression loading was performed at a 15 mm/sec deformation speed of up to 100% strain. The Young's modulus of the samples was determined as the slope in the linear elastic deformation region of the stress-strain graph. Therefore Young modulus at 60-95% strain [26] was calculated using the following formula:

$$\text{Young Modulus} : \frac{F \cdot L}{A \cdot \Delta L}$$

Where F stands for the uniaxial force applied to the surface of the scaffolds, A is the surface, ΔL is the height of the scaffolds after the force application and L is the initial height.

2.3. Evaluation of cytotoxicity and cell adhesion of cell-laden scaffolds

2.3.1. Cell culture maintenance

The MC3T3-E1 cells were used as a model system for the *in vitro* investigation of the viability and proliferation in the presence of the PEDOT:PSS/PVA/Gelatin scaffolds and PVA/Gelatin control scaffolds. The cells were cultured in alpha-MEM™ (PAN-Biotech, Germany) medium supplemented with 10% fetal bovine serum (FBS) (PAN-Biotech, Germany), 2 mM L-glutamine (PAN-Biotech, Germany), 100 µg/mL penicillin/streptomycin (PAN-Biotech, Germany), and 2.5 µg/mL amphotericin (fungizone) (Gibco, Thermo Fisher Scientific, UK), in a humidified incubator at 37 °C and 5% CO₂ (Heal Force, China). After reaching 80–90% confluence, the cells were harvested using trypsin/EDTA (Gibco, Thermo Fisher Scientific, UK). 5×10^3 cells were used for viability and proliferation assays, respectively, and were seeded onto the scaffolds. The medium was changed every three days. All experiments were carried out using cell passages from 6 to 8.

2.3.2. Cell viability evaluation by metabolic assay PrestoBlue™

The viability was determined by means of the resazurin-based PrestoBlue™ assay. When added to cells, the PrestoBlue™ reagent is modified by the reducing environment of the living cells. More specifically, the reagent is reduced from resazurin to resorufin which is red in color and highly fluorescent, therefore it can be measured photometrically. Conversion is proportional to the number of metabolically active cells. At each experimental time point (days 1, 3, and 7) in the cell culture, 10 µL of PrestoBlue™ reagent diluted in alpha-MEM™ at a ratio of 1:10 were added to each well and incubated at 37 °C for 60 min. The volume of 100 µL of the supernatants was transferred to a 96-well plate, and the absorbance was measured at 570 and 600 nm in a spectrophotometer (Synergy HTX Multi-Mode Microplate Reader, BioTek, Bad Friedrichshall, Germany). All samples were rinsed with PBS, and a fresh culture medium was added. The metabolic activity of living cells was correlated with cell numbers by means of a calibration curve. All samples were analyzed in eight replicates (n=8).

2.3.3. Cell adhesion and morphology

The surface morphology of the hydrogels as well as the adhesion and morphology of the MC3T3-E1 cells loaded onto them were observed by means of SEM (JEOL JSM-6390LV). Seeded scaffolds with 5×10^3 pre-osteoblastic MC3T3-E1 cells per sample, were cultivated in an incubator at 37 °C and 5% CO₂ for 7 days. On days 1, 3 and 7 of the experimental procedure, samples were removed from the incubator and were rinsed twice with PBS, fixed with 4% v/v paraformaldehyde (PFA) for 30 min, and dehydrated in increasing ethanol concentrations (30–100% v/v). The scaffolds were finally dried using Hexamethyl disilazane (HMDS) and left overnight to dry. After that the samples were sputter-coated with a 20 nm thick layer of Au (Baltec SCD 050) and observed under SEM (JEOL JSM-6390LV), at an accelerating voltage of 15kV.

2.4. Osteogenic response of MC3T3-E1 pre-osteoblastic cells under mechanical stimulation

2.4.1. Cell seeding of scaffolds prior mechanical stimulation

For the mechanical stimulation experiment, prior to seeding, all lyophilized scaffolds underwent sterilization through a 30 min exposure to UV radiation at a wavelength of 265 nm. Subsequently, the cells were seeded onto sterilized scaffolds at a density of 4×10^4 cells per scaffold and allowed to incubate for 1 h before additional culture medium was added, to facilitate the cell seeding process. After the initial cell attachment period, the medium was replaced with osteogenic medium, consisting of alpha-MEM™ supplemented with 10 nM dexamethasone (Sigma, USA), 10 mM β-glycerophosphate (Sigma, USA), and 50 µg/ml L-ascorbic acid 2-phosphate (Sigma, USA). The cell-loaded scaffolds were

cultured in this osteogenic medium for a specific duration and conditions to induce osteogenic differentiation.

2.4.2. Mechanical stimulation protocol

The experiment was performed according to a procedure described in a recently published report of our research group [36]. Briefly, each cell-seeded scaffold was subjected to mechanical force using a MechanoCulture TX (MCTX) bioreactor equipped with uniaxial cyclic compression (CellScale, Waterloo, Canada), a device that mimics the dynamic situation of the human body. The cell-loaded scaffolds underwent confined uniaxial compression, where the initial cell loading surface of the scaffolds was rotated by 90 degrees for mechanical stimulation as shown in Figure 2. Scaffolds were exposed to mechanical stimulation on their side, mimicking the direction of mechanical forces applied to bone and assuring that the cells cultured within the scaffolds experience compression forces during mechanical stimulation on their entire surface. The compression was applied at a frequency of 1 Hz and with a strain equivalent to 10% of the scaffold side (resulting in a displacement of 500 μm). Each compression cycle lasted for 1 hour and was performed daily, for a total duration of 21 days. The application of mechanical stress started the day after the addition of the osteogenic media, which was referred to as day 1 of the experiment. In order to compare the effects of dynamic (D) and static (S) conditions and further investigate the influence of mechanical stimulation on cell viability and differentiation, control static cultures were maintained under the same culture conditions without any mechanical stimulation.

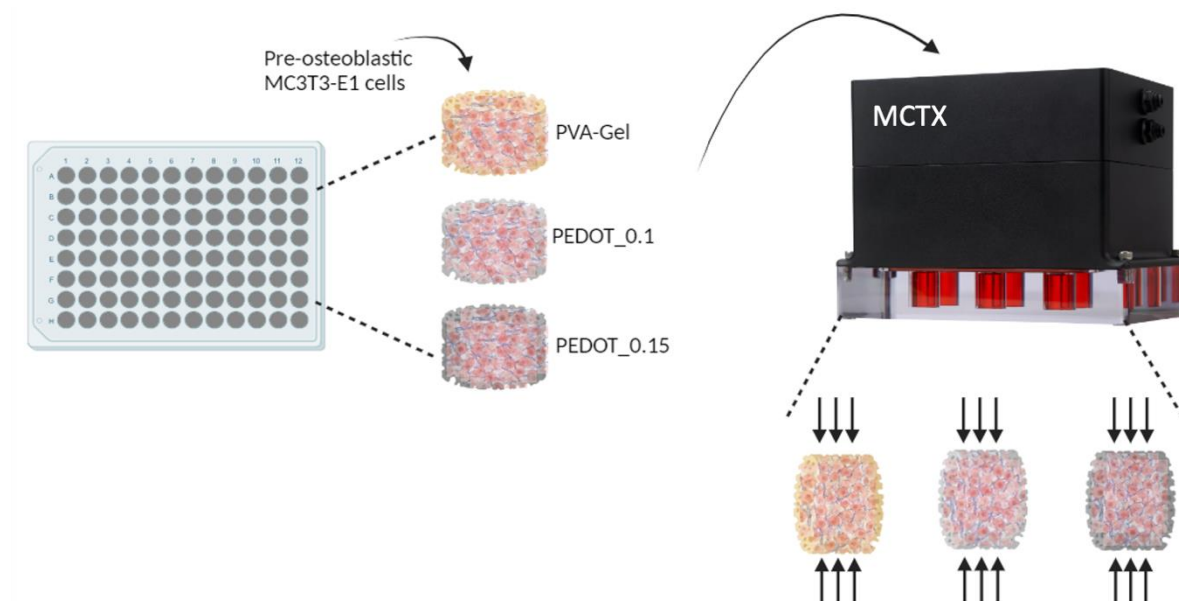


Figure 2. Schematic view of the experimental set up.

2.4.3. Cell viability of cell-laden scaffolds (constructs) via Live/Dead assay

Cell viability was assessed using a Live/Dead assay (Biotium, USA). This assay uses two fluorescent dyes, calcein AM (cal AM) and ethidium homodimer (EthD-1), to stain live and dead cells simultaneously. Briefly, the scaffolds of all compositions (n=3) after 3 and 7 days of culture were washed twice with PBS and then incubated in a working solution with 2 μM calcein acetoxymethylester (calcein AM) (494 nm excitation, 517 nm emission) and 4 μM ethidium homodimer III (EthD-III) (532 nm excitation, 625 nm emission) at room temperature for 30 min. Then, they were washed again with PBS, stored in culture medium, and imaged using a Confocal Laser Scanning Microscope (Leica TCS SP8). Cells were characterized as live when they fluoresced green after staining with calcein-AM and dead when they

fluoresced red after staining with EthD-III. Cells were imaged using a 1 μm step (z-axis) and adjusted to incorporate 100 μm height of the construct.

2.4.4. Determination of alkaline phosphatase (ALP) activity

Alkaline phosphatase, an enzyme that is prominent mainly at early osteogenic stages, was observed by confocal laser microscopy following staining. Live ALP stain generates a soluble phosphorylated molecule inside the cell that in presence of ALP yields a non-toxic green fluorescent product [37]. At predetermined time points, the cell-loaded scaffolds were subjected to ALP staining to assess osteogenic differentiation. The scaffolds were thoroughly washed with PBS and incubated with ALP staining (ThermoFisher, Alkaline Phosphatase Live Stain) solution for 1 h at 37 °C. Following staining, the scaffolds were rinsed with PBS and observed under a confocal microscope. Confocal images were acquired on days 3, 7, and 18 to visualize the distribution and intensity of ALP staining within the cell layer on the various scaffold compositions and conditions.

2.4.5. Calcium secretion measurements

Calcium secretion of the cell seeded scaffolds was determined by the O-cresol phthalein complexone (CPC) method (BIOLABO, Les Hautes Rives, French) [34]. In alkaline solution CPC reacts with calcium to form a dark-red colored complex. The absorbance measurements are proportional to the amount of calcium in the specimen. Calcium mineralization is one of the pivotal regulators for the formation of the ECM and is considered to be a late marker of osteogenesis. Briefly, supernatants were collected, and 10 μL from each were mixed with 100 μL of calcium buffer and 100 μL of calcium dye containing 78 $\mu\text{mol/L}$ CPC. Absorbance of the mixture was measured using a spectrophotometer (Synergy HTX Multi-Mode Microplate Reader, BioTek, Winooski, USA) at 550 nm. Absorbance values were correlated to calcium concentration by using a calibration curve. All samples were analyzed in quadruplicates (n=4).

2.4.6. Quantification of secreted collagen by cells within the constructs

Collagen type I is the most abundant component of the organic extracellular matrix of bone tissue and therefore its secretion and accumulation are a principal marker of the bone formation process [38]. The quantification of collagen secretion in the culture supernatants was performed using a standardized protocol of our research group that is based on the Sirius Red (PSP) staining method after 4,6,8,11,13,15,18 and 21 days in culture [39]. The PSR staining method relies on the elongated, anionic structure of the Sirius red dye molecule-binding parallel to cationic collagen fibers [40]. Briefly, at predetermined time points 25 μL of culture medium were diluted in 75 μL of ultrapure deionized water, mixed with 1 mL 0.1% w/v Sirius Red (Sigma, St. Louis, MO, USA) dye in 0.5 M acetic acid and finally incubated for 30 min at room temperature. After the centrifugation of samples at 15,000 g for 20 min at 4 °C, the scaffolds were washed with 0.5 M acetic acid to remove the non-bound dye. After the final centrifugation, 1 mL of a 0.5 M NaOH solution was added to extract the collagen bound dye complex and measured in a spectrophotometer (Synergy HTX Multi-Mode Microplate Reader, BioTek, Winooski, USA). 200 μL of each solution were transferred to a 96-well plate and the measurements were taken at 530 nm. The absorbance values were correlated to $\mu\text{g/mL}$ of collagen by using a calibration curve. All samples were analyzed in quadruplicates (n=4).

2.4.7. Energy dispersive spectroscopy (EDS) analysis

Scanning electron microscopy (SEM) was employed to visualize the calcium and phosphorus biomineralization within the scaffold. For the preparation of the samples a well-established protocol of our research group was followed [41]. Briefly, the samples were rinsed twice with PBS, fixed with 4% v/v PFA for 30 min, and dehydrated in increasing ethanol concentrations (30-100% v/v). Afterward,

the samples were dried using HMDS and left overnight to dry. Following the samples were sputter-coated with a 20 nm thick layer of Au (Baltec SCD 050) and observed under SEM (JEOL JSM-6390LV), at an accelerating voltage of 15 kV. EDS analysis was performed to determine the elemental composition of the biomineralized regions observed through SEM imaging. The EDS detector integrated within the SEM system collected X-ray spectra emitted by the samples upon electron beam interaction. The acquired spectra were analyzed to identify the presence and relative abundance of calcium and phosphorus, enabling quantitative and visualized assessment of biomineralization. The SEM images allowed the observation of the spatial distribution of calcium and phosphorus biomineralization onto the scaffold surface. The EDS analysis provided quantitative information on the elemental composition, allowing the determination of calcium and phosphorus ratios in the biomineralized regions.

2.4.8. X-ray diffraction (XRD) analysis

XRD was employed to evaluate the HA composition in the scaffold. To perform this analysis, the scaffolds were first freeze-dried for 24 h for water removal and consequently avoiding excess background noise on the final graph. XRD analysis was performed by the triple axis in a high-resolution X-ray diffractometer (HR-XRD) BEDE D1 with Cu K α radiation ($\lambda=1.5460$ Å), operating at 45 kV and 40 mA, for an angle step of 0.0241° and 2 θ range from 20 to 60°. The instrument was equipped with a suitable X-ray source and a detector capable of capturing diffracted X-rays. The samples were exposed to X-rays, and the resulting diffraction patterns were recorded. The obtained XRD patterns were analyzed using GraphPad Prism version 8 software to determine the composition of HA in the scaffold. The diffraction peaks were compared with those of the HA standard to confirm the presence of characteristic HA peaks. The positions and intensities of the peaks were used to identify the HA crystallographic phases and assess the degree of crystallinity. The accuracy and reliability of the XRD analysis were ensured by performing two replicates (n=2) of the measurements. Control, and background subtraction, were conducted to account for any instrumental artifacts or background noise that any residue of humidity in the scaffolds could have created.

2.5. Statistical analysis

Statistical analysis was performed for the Young's modulus, % swelling ratio, % mass loss, electrical conductivity cell viability, calcium and collagen secretion assessment using the two-way ANOVA Dunnett's multi-comparison test in GraphPad Prism version 8 software (GraphPad Software, San Diego, CA, USA). P-values indicate statistically significant differences. Single symbols (*) or (#) show statistically significant differences with $p<0.05$, two symbols (**) or (##) designate $p<0.01$, three symbols (***) or (###) indicate $p<0.001$, four symbols (****) or (####) indicate $p<0.0001$ and five symbols (*****) or (#####) are for $p<0.00001$.

Chapter 3. Results

3.1. Physicochemical and mechanical characterization of scaffolds

3.1.1. Scaffolds' morphology at macroscopic and microscopic view

The bioengineered scaffolds compositions as well as concentrations and crosslinking method are displayed in Table 1. All scaffolds were fabricated through lyophilization and had a diameter of approximately 5 ± 0.05 mm and a height of 14 ± 0.05 mm. They all resemble sponge-like structures with different shades of black depending on their consistency (Fig. 1). Crosslinked scaffolds, as well as scaffolds containing higher concentrations of PEDOT:PSS appear to be darker than the others. Control PVA/Gelatin scaffolds were white. Pores are detectable on all scaffolds macroscopically.

Table 1. Acronyms of the various scaffold compositions. PEDOT:PSS is the acronym for poly(3,4-ethylene dioxythiophene):poly(styrene sulfonate), PVA is the acronym for poly(vinyl alcohol), and GOPS is the acronym for (3-glycidyloxypropyl)trimethoxysilane

Scaffold acronyms	Composition
PVA-Gel	5% w/v PVA and 5% w/v gelatin, without PEDOT:PSS, serves as control
PVA-Gel_C	5% w/v PVA and 5% w/v gelatin, without PEDOT:PSS, crosslinked with GOPS and 0.025% w/v glutaraldehyde, serves as control
PEDOT_0.1	0.10% w/v PEDOT:PSS, 5% w/v PVA and 5% w/v gelatin
PEDOT_0.1_C	0.10% w/v PEDOT:PSS, 5% w/v PVA and 5% w/v gelatin, crosslinked with 2% v/v GOPS and 0.025% w/v glutaraldehyde
PEDOT_0.15	0.15% w/v PEDOT:PSS, 5% w/v PVA and 5% w/v gelatin
PEDOT_0.15_C	0.15% w/v PEDOT:PSS, 5% w/v PVA and 5% w/v gelatin, crosslinked with 2% v/v GOPS and 0.025% w/v glutaraldehyde

3.1.2. FTIR spectra analysis

FTIR spectra are a useful tool to identify the presence of certain functional groups in a molecule as each specific chemical bond often has a unique energy absorption band. To better understand the bond formation and to detect the crosslinked structure and intermolecular interactions, we acquired the FTIR spectra of all scaffold types as well as their basic components in the range of 4000 cm^{-1} to 500 cm^{-1} wavelengths. The results are presented in the Figure 3. For pure gelatin we observed prominent bands corresponding to amide A, amide B, amide I, amide II and amide III regions [42]. The amide A band arises between $3200\text{--}3500\text{ cm}^{-1}$ where the stretching vibrations of N-H bonds can be found. At the same region O-H bonds are present. Also, a peak around 3100 cm^{-1} is related to the asymmetric stretching of C-H bonds, associated with amide B. Moreover, there is an intense peak at $1600\text{--}1700\text{ cm}^{-1}$ which indicates the presence of C=O bonds, attributed to amide I. The amide II band typically observed at $1500\text{--}1600\text{ cm}^{-1}$ arises a peak attributed to the combination of N-H bending and C-N stretching vibrations. Finally, regarding the amide III, a peak at $1200\text{--}1300\text{ cm}^{-1}$ corresponds to the deformation of N-H bonds and the bending of C-N bonds [34]. Pure PVA exhibits a broad peak between $3200\text{--}3500\text{ cm}^{-1}$, indicating the stretching vibrations of -OH hydroxyl groups. Nearby a peak at $2850\text{--}3000\text{ cm}^{-1}$ due to C-H alkyl stretching, can be found. The carbonyl group C=O stretching vibrations occur

around at 1750 cm^{-1} . Furthermore, a peak at 1450 cm^{-1} and 1350 cm^{-1} associated with the C-H and O-H bending respectively. In addition, a peak at 1100 cm^{-1} is observed attributed to the C-O deformation [43, 44]. Pure PEDOT: PSS had a prominent band at $3200\text{--}3500\text{ cm}^{-1}$, indicating the stretching vibrations of -OH hydroxyl groups of PSS. C-C and C=C stretching of the aromatic rings of PSS are represented by the spikes at around 1650 cm^{-1} , whereas the peak at 1190 cm^{-1} reveals a symmetric stretching of the PSS S=O band. Also, a peak at 1090 represents the C-O-C stretching vibration band of PEDOT ring. Finally, mild peaks were seen at 1200 cm^{-1} and 960 cm^{-1} corresponding to the stretching vibration of SO_4H group of PSS and to the C-S bonds in the thiophane ring of PEDOT [45, 46]. Similar peaks are evident in all types of PEDOT:PSS-containing scaffolds with small changes in the spectrums of PVA/Gelatin control scaffolds. All crosslinked PEDOT:PSS-containing scaffolds have the characteristic deep peak of pure PEDOT:PSS at $3200\text{--}3500\text{ cm}^{-1}$, validating the crosslinking between PVA-Gelatin matrix and PEDOT:PSS. On the other side, the non-crosslinked scaffolds appear to have a milder peak at the same region, confirming that the binding of the PEDOT:PSS was weaker. As for the control PVA/Gelatin scaffolds, most of the peaks of their basic components are present, verifying a well-established bonding between those groups and the different charged groups of Gelatin (positive) [47] and PVA (negative) [48]. No significant differences between crosslinked and non-crosslinked control scaffolds are observed.

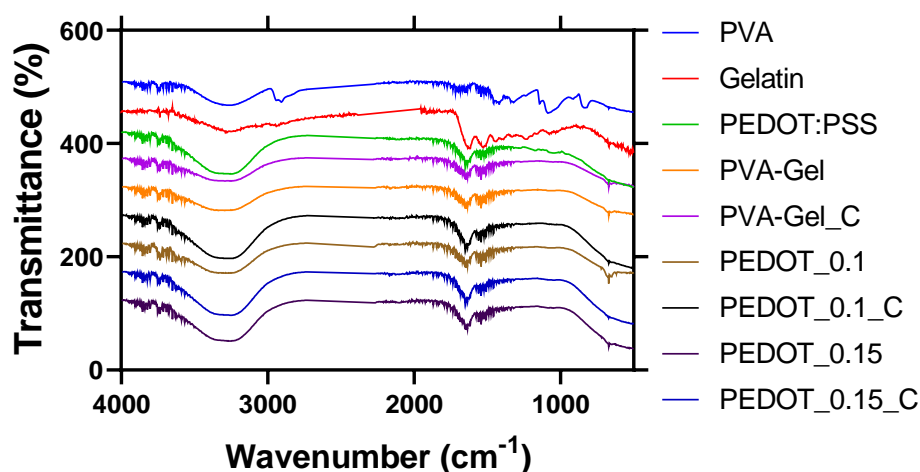


Figure 3. FTIR spectra of the different scaffold types and their basic components, PVA, gelatin, PEDOT:PSS. 'C' designates crosslinked scaffolds.

3.1.3. Degradation analysis

Degradation rates for the various scaffold compositions after 4, 7, 14, 21 and 28 were observed and are demonstrated in Figure 4. PVA-Gel and PVA-Gel_C scaffolds possessed the higher degradation rates. PEDOT_0.1 had significantly lower degradation values compared to the corresponding PVA-Gel control scaffolds, for all time points. The same pattern is documented for the PEDOT_0.15 scaffolds as well. Conversely, for the crosslinked scaffolds, PEDOT_0.1_C had significantly lower values than the corresponding control PVA-Gel_C scaffold at all time points. Similar tendency is being recorded for the PEDOT_0.15_C. In general, PEDOT:PSS-containing scaffolds had maintained their initial weight and integrity for longer period of time in culture conditions. Therefore, preserving mechanical integrity through controlled degradation is particular important in load-bearing areas such as the human cartilage where the scaffold needs to withstand mechanical forces during the healing process [49].

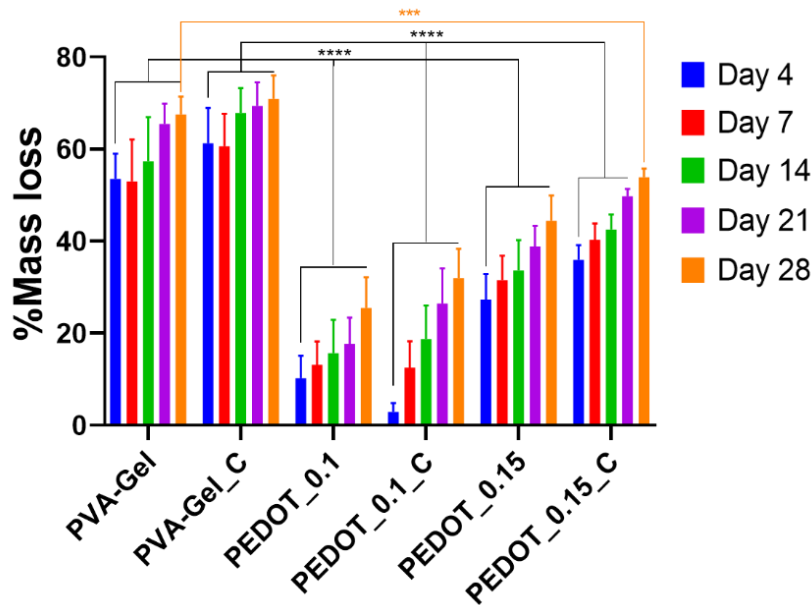


Figure 4. Degradation rates of the different scaffold compositions on days 4,7,14,21 and 28. The presence of PEDOT:PSS led to a significant reduction of degradation rates from $70.0 \pm 5.1\%$ to $50.0 \pm 5.5\%$. (* $p < 0.05$, ** $p < 0.01$, *** $p < 0.001$, **** $p < 0.0001$, denotes a statistically significant difference compared to the corresponding control scaffold.)

3.1.4. Swelling ratios

The scaffolds absorbed the maximum amount of PBS in 15 min. After 24 h freeze-drying, their weight was measured. Both crosslinked and non-crosslinked scaffolds possessed the ability to swell. Liquid uptake is exhibited in Figure 5. PEDOT_0.15_C scaffold had a slightly better ability to absorb ($88.0 \pm 2.4\%$) PBS in comparison with the PEDOT_0.15 scaffold ($82.0 \pm 7.1\%$). Significant differences had the PEDOT_0.15_C ($88.0 \pm 2.4\%$) compared with the respective control PVA-Gel_C ($63.0 \pm 7.5\%$) as well as the PEDOT_0.15 ($82.0 \pm 7.1\%$) with the PVA-Gel ($49.0 \pm 8.0\%$).

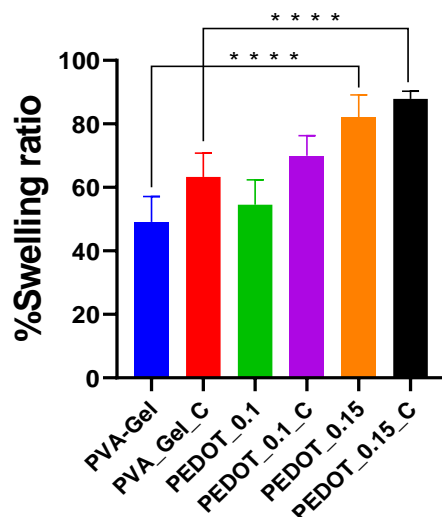


Figure 5. Swelling ratios of the lyophilized scaffolds after 3 h immersion in PBS. The presence of PEDOT:PSS led to a significant increase in swelling ratio from $49.0 \pm 8.0\%$ to $88 \pm 2.4\%$. (* $p < 0.05$, ** $p < 0.01$, *** $p < 0.001$, **** $p < 0.0001$, denotes a statistically significant difference compared to the corresponding control scaffold.)

3.1.5. Porosity of scaffolds

Porosity of all scaffolds is demonstrated through SEM images at three different magnifications, 50 x, 200 x and 1000 x (Fig. 6A) Porosity was quantified via the SEM images using ImageJ (Fig 6B) and through the liquid displacement method using water as shown in Figure 6C. PEDOT:PSS-containing scaffolds demonstrated higher porosity levels in comparison with the control scaffolds. More specifically, PEDOT_0.15_C has the greatest value of $57 \pm 1.6\%$ porosity exceeding the value of PEDOT_0.15 ($54 \pm 2.0\%$). The same pattern is applied on the PEDOT_0.1 scaffolds with the crosslinked one slightly exceeding the non-crosslinked. PVA-Gel control scaffolds proved to have fewer pores overall with an average % porosity of $12 \pm 3.4\%$, whereas the addition of PEDOT:PSS presents a tendency to significantly increase porosity. Furthermore PEDOT_0.15_C and PEDOT_0.1_C exhibited the most well-defined pores compared to the other types.

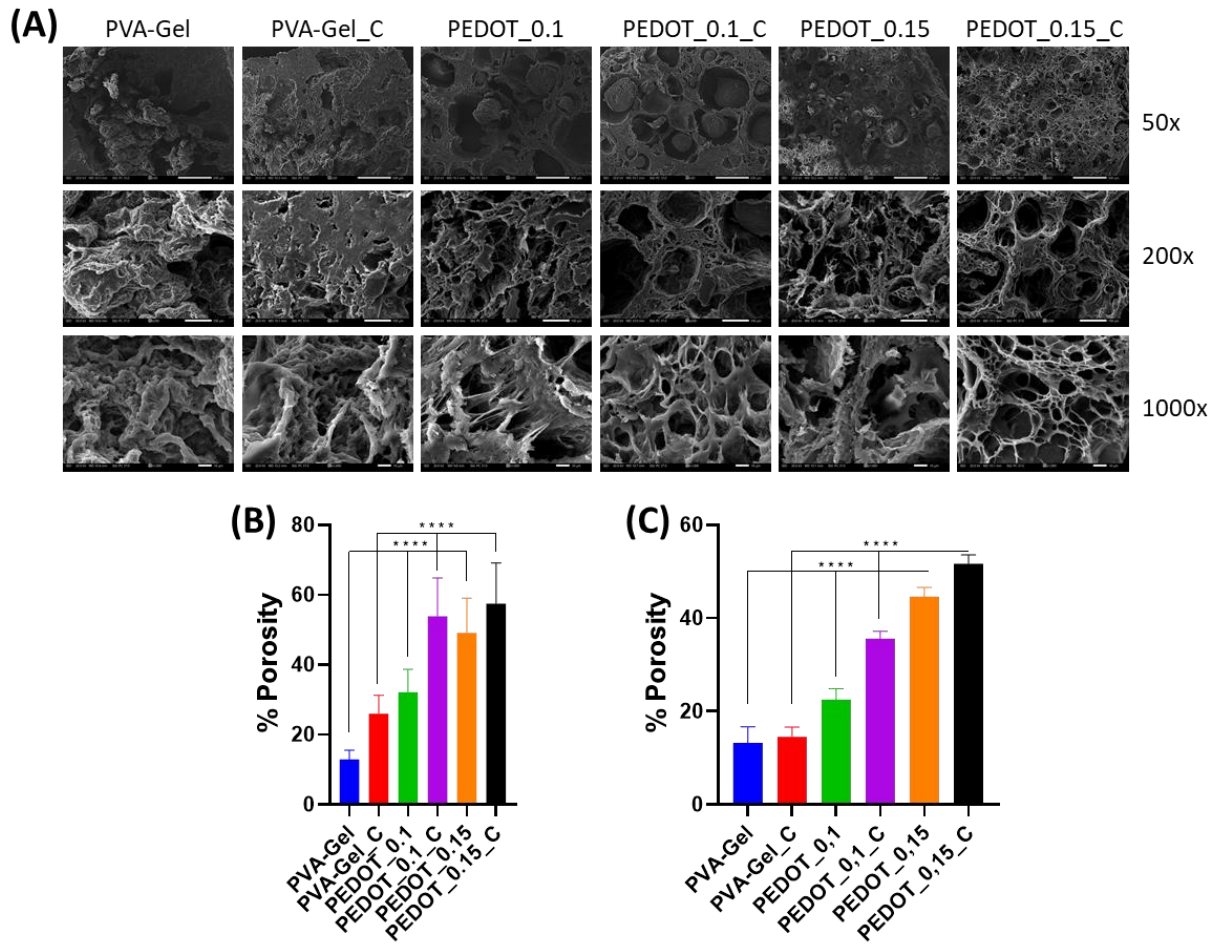


Figure 6. The porosity of all scaffold compositions is depicted via SEM in three magnifications (50x first panel, 200x second panel and 1000x third panel) (A). PEDOT_0.15_C indicates the most well-defined pores. The scale bar represents 500 μm , 100 μm , 10 μm respectively. Evaluation of % porosity calculated via SEM images using ImageJ (B) and through the liquid displacement method (C). Crosslinked scaffolds present higher porosity values than the non-crosslinked with the exception of the PVA-Gel (control) scaffolds, which exhibit fewer pores. Each bar represents the mean \pm SD of seven replicates. (* $p < 0.05$, ** $p < 0.01$, *** $p < 0.001$, **** $p < 0.0001$, denotes a statistically significant difference compared to the corresponding control scaffold.)

3.1.6. Electrical conductivity

The electrical conductivity is shown in Figure 7. It can be observed that the PEDOT:PSS-containing samples demonstrated significantly higher conductivity values compared to the PVA/Gel control composition ($621 \pm 10 \text{ Ms/cm}$). This suggests that the incorporation of PEDOT:PSS into the scaffold material substantially enhanced its electrical conductivity. PEDOT_0.15 exhibits the highest conductivity ($1047 \pm 24 \text{ } \mu\text{S/cm}$), however, when comparing PEDOT_0.1 ($1015 \pm 4 \text{ } \mu\text{S/cm}$) and PEDOT_0.15, no statistically significant differences between them are evident.

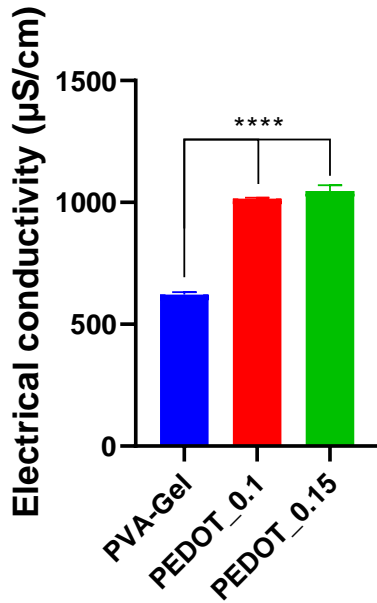


Figure 7. Evaluation of the electrical conductivity of the three compositions. The presence of PEDOT:PSS led to a significant increase in electrical conductivity. Each bar represents the mean \pm SD of seven replicates. (* $p < 0.05$, ** $p < 0.01$, *** $p < 0.001$, **** $p < 0.0001$, denotes a statistically significant difference compared to the PVA-Gel control sample).

3.1.7. Evaluation of the scaffolds' mechanical properties

The elastic modulus was measured at range of 65-95% strain [26], at a velocity of $15 \pm 0.05 \text{ mm/sec}$. The scaffolds were measured when hydrated in order to provide an approximation of the pressure that the materials can withstand in a liquid environment such as the human body. In Figure 8 the results are presented. The mechanical tests indicated that the Young modulus of the PEDOT_0.15_C ($3.4 \pm 0.9 \text{ MPa}$) scaffold was significantly greater compared to PVA-Gel_C control scaffold ($1.7 \pm 0.5 \text{ MPa}$) while the PEDOT_0.1_C had comparable values with the control. Moreover, for the non-crosslinked scaffolds PEDOT_0.1 ($2.4 \pm 0.2 \text{ MPa}$) as well as PEDOT_0.15 ($2.7 \pm 0.2 \text{ MPa}$) had significantly higher values than the PVA-Gel scaffold. Of note, scaffolds maintained good structural integrity throughout 21 days in culture media, confirming scaffold stability under physiological conditions. No major swelling or morphological changes were observed (data not shown).

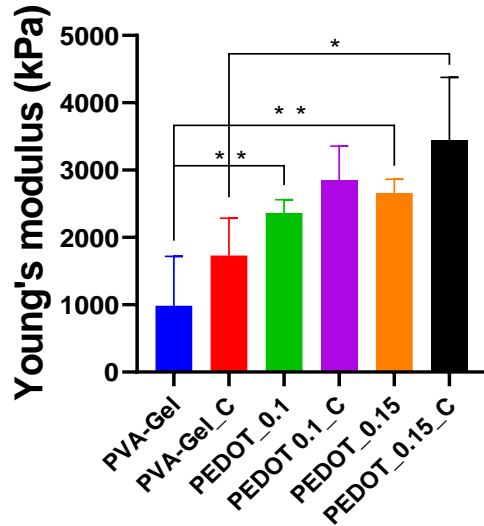


Figure 8. Evaluation of elastic modulus of the scaffolds at 60-95% strain, at a 15 ± 0.05 mm/sec velocity. PEDOT:PSS/PVA/Gelatin scaffolds presented favorable mechanical properties for bone tissue engineering. Their elastic modulus ranged between 1 and 5 MPa.

3.2. Evaluation of cell adhesion, morphology, viability and proliferation within scaffolds

3.2.1. Viability and proliferation of pre-osteoblastic cells within the scaffolds

The cell viability and proliferation of the pre-osteoblastic cells in the different hydrogels was quantitatively assessed after 1, 3 and 7 days in the culture. The corresponding graph is depicted in Figure 9A, 9B. All hydrogel types formed a gradual rate of increase in cell numbers over an incubation period of 7 days. At day 3 most samples exhibit a statistically significant increase in cell population, compared to the control, indicating an upregulated proliferation potential of MC3T3-E1 cells on the hydrogels. PEDOT_0.1 had similar absorbance values on day 3 and 7, while PEDOT_0.15 exhibits significant increase at day 7. PEDOT_0.1_C appears to have the lowest signals out of all different types, while PEDOT_0.15_C exhibits high absorbance values on day 3 and 7 but still lower than the PEDOT_0.15. This may be attributed to the crosslinking procedure. Overall, the pre-osteoblastic cell proliferation and growth within the biomaterial, validated that all scaffold compositions have excellent biocompatibility. The results from the cell viability assessment are in line with the findings from the SEM analysis, which are indicative of the cell adhesion and proliferation capabilities of pre-osteoblastic cells when loaded onto the scaffolds.

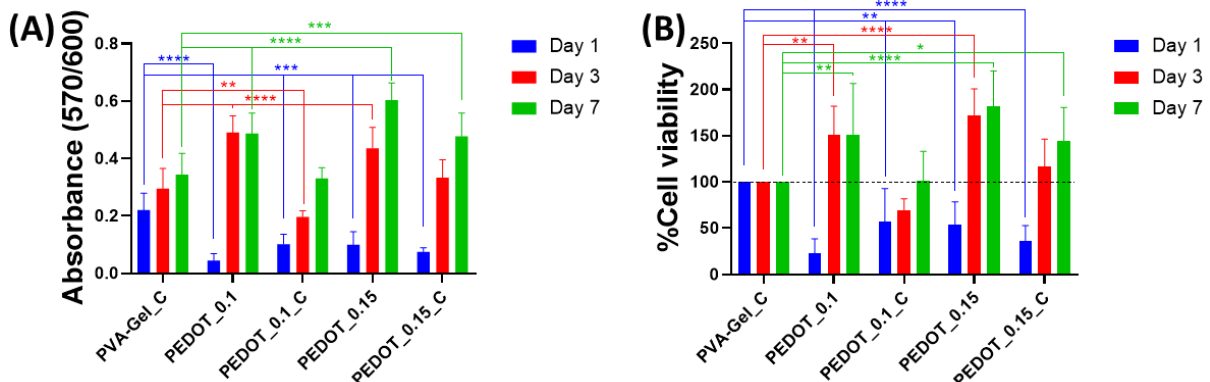


Figure 9. Cytotoxicity assessment on days 1, 3 and 7 expressed as absorbance values (A). % Cell viability (B). All scaffolds exhibit great biocompatibility, with the PEDOT_0.15 slightly exceeding the other compositions. (* $p < 0.05$, ** $p < 0.01$, *** $p < 0.001$, **** $p < 0.0001$, denotes a statistically significant difference compared to the PVA-Gel_C control scaffold at the corresponding time point).

3.2.2. Cell adhesion and morphology of pre-osteoblastic cells within the scaffolds

Representative SEM images (Fig. 10) display the adhesion of pre-osteoblastic cells within the various scaffold compositions after 1 day in culture. All SEM images are taken at 1000 × magnification and the scale bar represent 10 µm. Cells represent their characteristic elongated morphology on all PEDOT:PSS-containing hydrogels and protrusions for cell–cell interactions that are expected to promote tissue formation. Cell infiltration within the pores of the hydrogels was observed. Specifically, PEDOT_0.1 and PEDOT_0.15 present the most well adhered and elongated cells, followed by the PEDOT_0.15_C scaffold. PVA-Gel-C scaffolds appear to have fewer adhered cells, not as elongated as the other PEDOT-containing scaffolds. Similar images are those of PEDOT_0.1_C, with well spread cells but not as many as the other scaffold compositions. Unseeded scaffolds images are also shown for comparison purposes as they served as a reference point to highlight the presence and distribution of cells. With this approach, it was possible to distinguish the cells from the biomaterial and have a better view of the cell morphology.

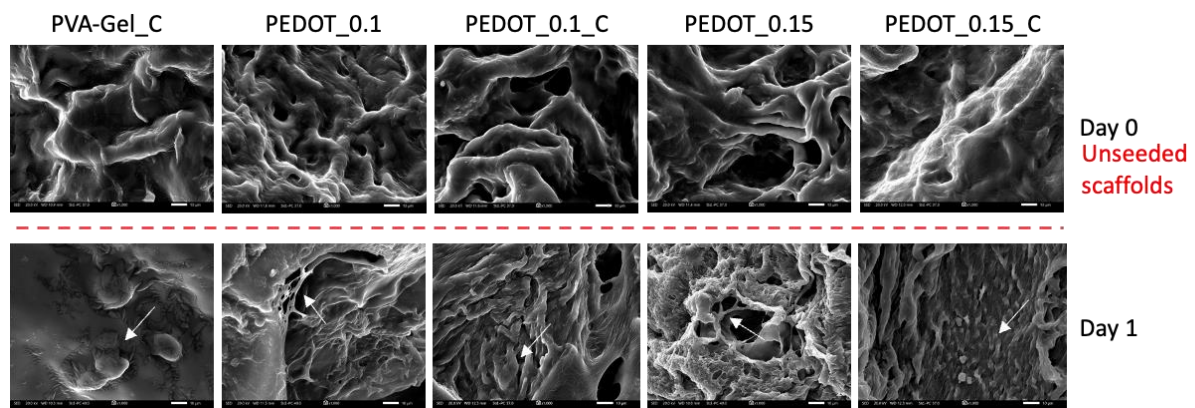


Figure 10. Representative SEM images showing the morphology of pre-osteoblastic cells seeded onto the different scaffold compositions after 1 day in culture. Unseeded scaffolds images are shown in the upper panel for comparison purposes. The white arrows point to the adhered cells. The scale bar represents 10 µm.

3.3. Osteogenic response of MC3T3-E1 pre-osteoblastic cells on the piezoelectric scaffolds under mechanical stimulation

3.3.1. Morphology of pre-osteoblastic cells within the constructs

The morphology of pre-osteoblastic cells onto the different type of scaffolds was visualized using SEM on days 7 and 14 of the experiment. All SEM images are taken at 1000 × magnification and the scale bar represent 10 µm and are shown in Figure 11. The acronyms of each composition and the experimental conditions are displayed in Table 2. Cells adhered well to the scaffold’s surface and exhibited their distinct elongated morphology with an increasing proliferation rate up to day 14. More specifically, for the dynamic condition, at day 7, all scaffolds appear to have an extended cell proliferation and adhesion. PEDOT_0.15_D and PEDOT_0.15_C_D presents well spread cells with some cells already formed pseudopodia. At day 14, cell adhesion and cytoskeletal organization were found to be enhanced on the biomaterial, indicating a favorable cellular response. Cells have covered most of the scaffolds’ surfaces, revealing a dense cell sheet formed by fully spread-out pre-osteoblasts. This observation is verifying the excellent biocompatibility of the scaffolds.

Table 2. Acronyms of the various scaffold compositions and the experimental conditions static (S) and dynamic (D). Non-crosslinked PVA-Gel scaffolds were not stable in culture conditions and consequently not employed in the experiments. (D) indicates the conditions performed using a mechanical stimulation protocol as described in section 2.4.2.

Scaffold acronym		Experimental condition (static/dynamic)
PVA-Gel_S	-	
PVA-Gel_D	-	
PVA-Gel_C_S		PVA-Gel_C under static culture condition
PVA-Gel_C_D		PVA-Gel_C under dynamic condition
PEDOT_0.1_S		PEDOT_0.1 under static culture condition
PEDOT_0.1_D		PEDOT_0.1 under dynamic condition
PEDOT_0.1_C_S		PEDOT_0.1 under static culture condition
PEDOT_0.1_C_D		PEDOT_0.1 under dynamic condition
PEDOT_0.15_S		PEDOT_0.15 under static culture condition
PEDOT_0.15_D		PEDOT_0.15 under dynamic condition
PEDOT_0.15_C_S		PEDOT_0.15 under static culture condition
PEDOT_0.15_C_D		PEDOT_0.15 under dynamic condition

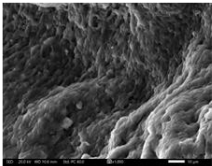
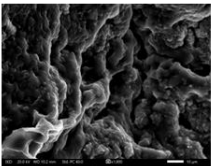
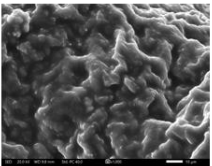
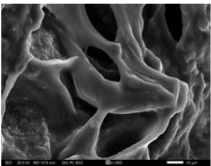
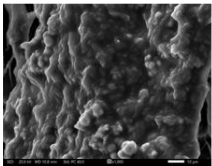
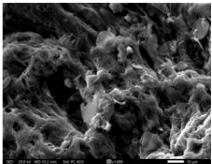
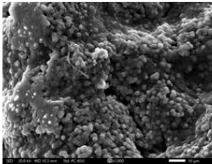
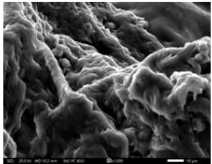
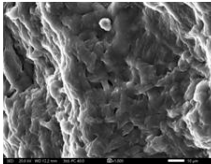
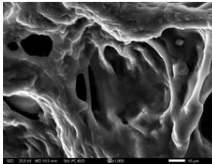
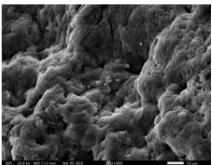
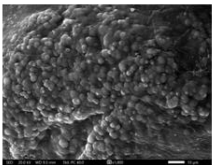
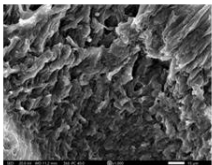
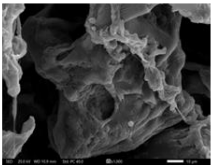
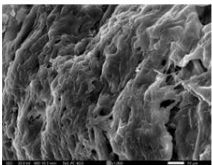
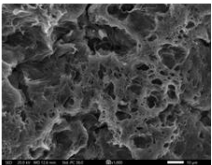
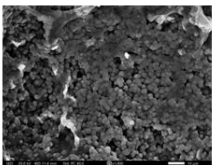
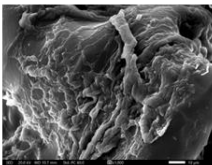
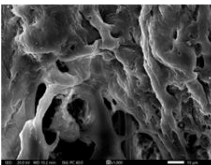
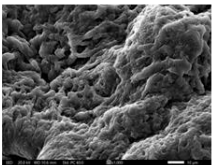
	PVA-Gel_C	PEDOT_0.1	PEDOT_0.1_C	PEDOT_0.15	PEDOT_0.15_C	
Static						Day 7
Dynamic						
Static						Day 14
Dynamic						

Figure 11. Representative SEM images showing the morphology of pre-osteoblastic cells seeded onto the different scaffold compositions after 7 and 14 days. The scale bar represents 10 μm

3.3.2. Live/Dead assay

In order to investigate the viability of the seeded MC3T3-E1, scaffolds were cultured for 7 days. On day 3, live and dead cells were simultaneously stained with calcein AM and EthD-1 which showed the images of live (stained green) and dead (stained red) cells (Fig. 12). Images reveal that for all five concentrations and over the whole culture period, majority of the cells survived the protocol and cultivation process. Specifically, cells that survived in the dynamic culture seems to be significantly higher compared to the static one.

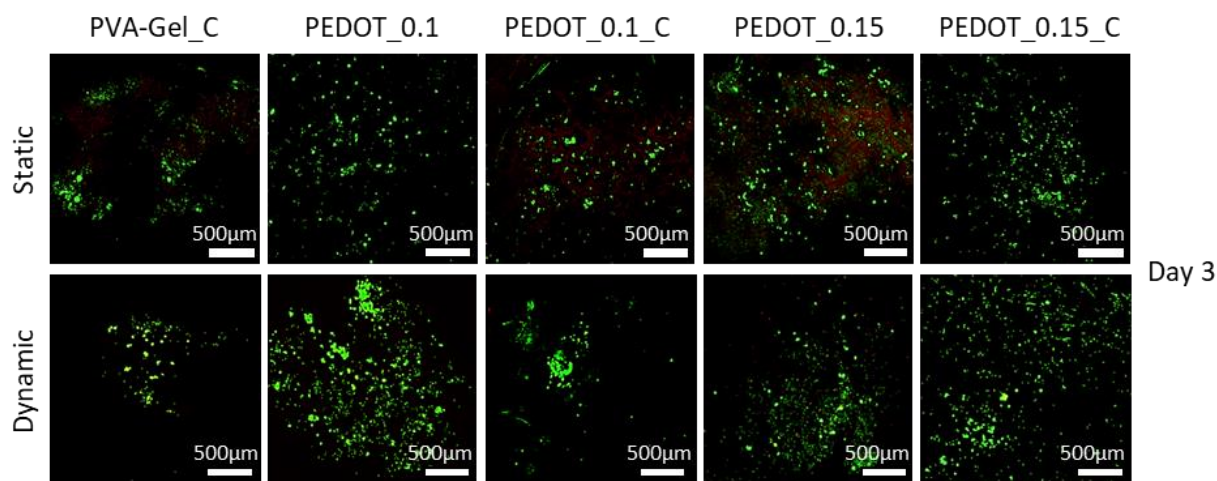


Figure 12. Cytotoxicity assessment on day 3 via confocal scanning microscopy. Live cells are shown in green and dead cells are shown in red. The scale bar represents 500 μm .

3.3.3. Determination of the alkaline phosphatase activity

ALP is commonly used as an early marker for osteogenic differentiation and can be assessed through various methods including biochemical assays and staining techniques. In this study it was evaluated through a staining protocol and visualized via confocal microscopy. Corresponding images of the ALP expression are evident in Figure 13. Three pre-determined time points were examined: day 3, day 7 and day 18. At day 3 PEDOT_0.15_C_D displayed significantly higher ALP activity levels compared to the other compositions, followed by PEDOT_0.1_C_D. The same trend is being observed in the subsequent time points, albeit with a less highlighted effect as the ALP is an early marker and it is expressed more in primitive time points. All dynamic culture conditions were superior compared to the static control at this particular time point. In conclusion, the incorporation of PEDOT:PSS into PVA/Gelatin matrix was proved to be vital for the osteogenic differentiation, with the scaffolds containing higher PEDOT:PSS concentrations showing the highest values. Especially, crosslinked scaffolds that formed stronger bonds between the materials and have successfully integrated PEDOT:PSS into the matrix demonstrated higher levels of ALP activity. These findings highlight the influence of PEDOT:PSS as a piezoelectric material that responds to mechanical stimulation by producing electrical signals, thereby triggering the opening of voltage-gated calcium channels and inducing osteogenic differentiation [17].

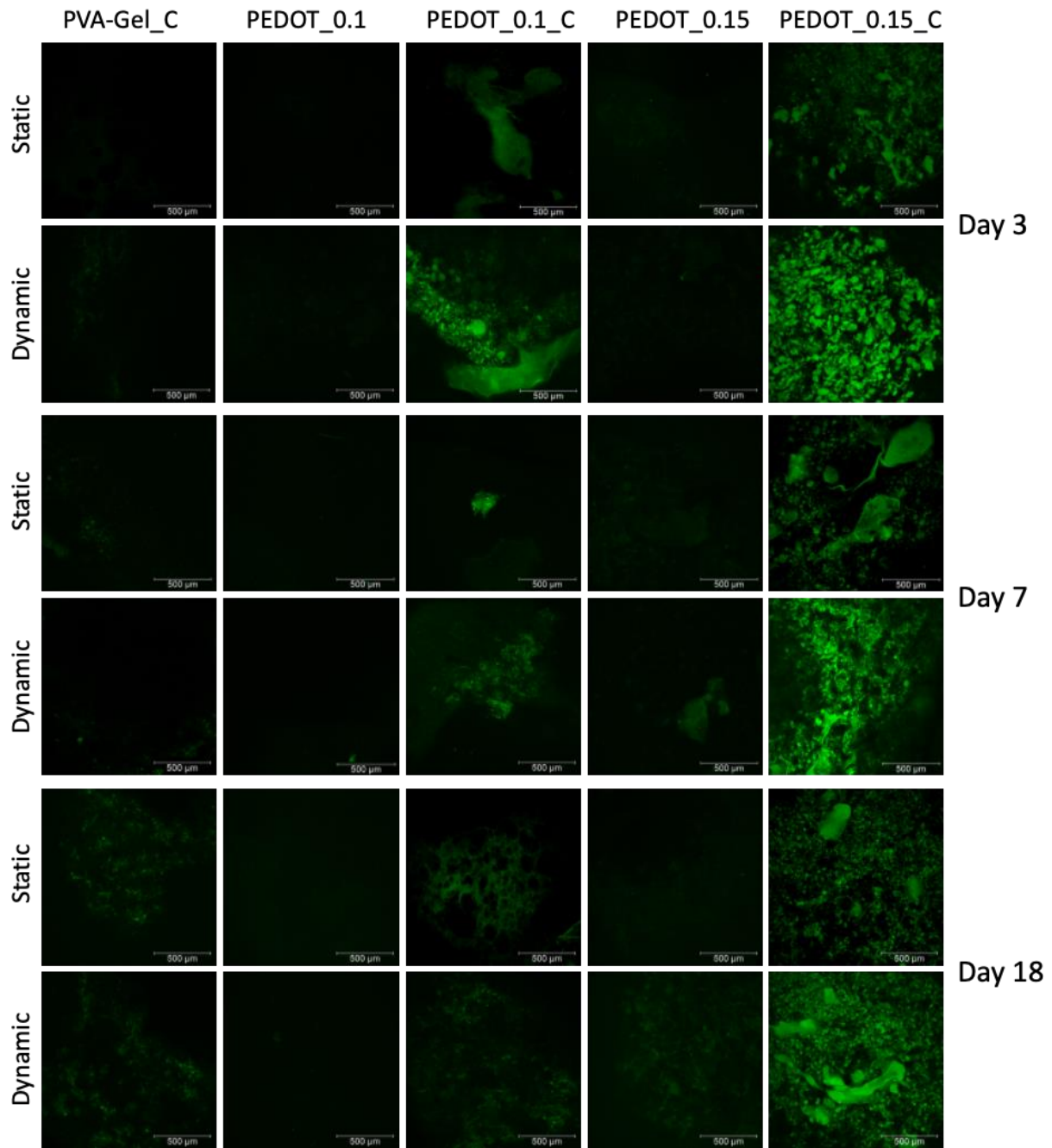


Figure 13. ALP activity on days 3, 7 and 18 observed by confocal laser scanning microscopy following live staining (green). The scale bar represents 500 μm.

3.3.4. Calcium secretion measurement

Calcium deposition is a marker that signifies bone formation and its presence indicates the shaping of bone-like structures. With the quantification of calcium concentration in the culture medium, level of osteoblastic activity and mineralization is evaluated [50]. Calcium levels for the different scaffolds are presented in Figure 14A. The results indicate that there is a consistent and steady increase in calcium concentration over time in all scaffolds, implying continuous differentiation of pre-osteoblasts into mature osteoblasts until day 21. Notably, the scaffolds subjected to mechanical stimulation exhibited higher values, suggesting that mechanical stimulation enhances the differentiation potential. Particularly, the compositions with the greater values were PEDOT_0.15_D, PEDOT_0.15_C_D and PEDOT_0.1_D. Both the activity of ALP and the production of calcium support this finding, signifying

that the PEDOT:PSS-containing scaffolds subjected to mechanical stimulation have a greater differentiation capacity compared to the non-stimulated ones. It is worth noting that mechanical stimulation does not negatively impact the osteogenic potential but rather further promotes it.

3.3.5. Collagen secretion quantification

Collagen type I is a vital constituent and the most abundant organic component of bone tissue that serves a structural role in the ECM formation [51]. Collagen concentration was quantified in the supernatants as a middle marker of osteogenesis. Cell supernatants were collected after 4,6,8,11,13,15,18, and 21 days of the experiment. The evaluation of collagen concentration (Fig. 14B) revealed a universal increase. The scaffolds depicted comparable collagen levels production under both dynamic and static culture conditions. Collagen level secreted by pre-osteoblasts on the various types of scaffolds, demonstrated a threefold increase from day 7 to day 14. A slight decrease in the rate of collagen production was observed after 13 days in culture, especially for the static condition. By day 21, all mechanical stimulated scaffolds indicated higher levels of collagen concentration compared to the static equivalent, with PEDOT_0.15_C_D retaining the highest values.

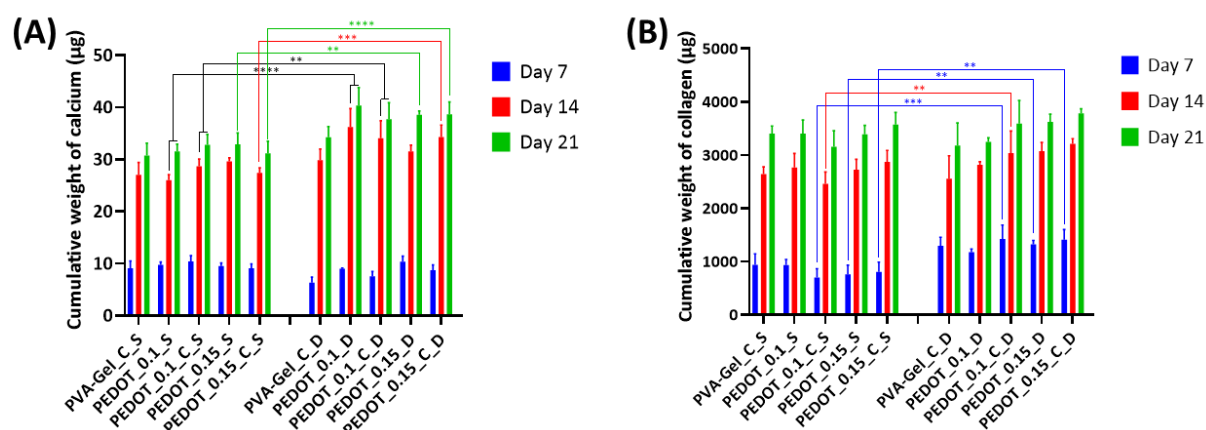


Figure 14. Levels of calcium on days 7, 14, and 21, depicted by graph bars (A). Levels of collagen on days 7, 14, and 21, described by graph bars (B). S' designates static culture, 'D' dynamic culture (under mechanical stimulation), and 'C' crosslinked. (*p<0.05, **p<0.01, ***p<0.001, ****p<0.0001, denotes a statistically significant difference between static and dynamic culture at the corresponding time point.)

3.3.6. Energy dispersive spectroscopy (EDS) analysis of biomineralization

EDS analysis was carried out for all different scaffold compositions and time points using a SEM (JEOL JSM-6390LV), in order to determine the existence of the element's composition on the surface of the hydrogels. Previously, SEM images were obtained showing the biomineralization on the surface of the scaffolds. Remarkably, the EDS analysis revealed the presence of significant calcium and phosphorous deposition for various scaffolds. Specifically, as shown in Figure 15A at day 7 only PEDOT_0.15_C_D demonstrated evidence of calcium deposition. At day 14 in dynamic culture three of the five scaffolds exhibited calcium deposition, PEDOT_0.1_C_D, PEDOT_0.15_D and PEDOT_0.15_C_D. These results are in line with the previous examined osteogenic markers, highlighting the key role of PEDOT:PSS as a component that promotes osteogenesis. At day 21, calcium deposition is presented onto all scaffolds. Regarding phosphorous, biomineralization is being observed in all scaffolds at day 21 in contrast with day 14 that phosphorous is presents only in PEDOT_0.1_C_D and PEDOT_0.15_C_D (Fig. 15B). The identification of these elements is highly indicative of biomineralization, a fundamental process for the formation of mineralized tissues such as bone. The presence of calcium and phosphorous suggests the potential creation of HA, a major component of natural bone. In that notice, Ca/P ratios were

evaluated via EDS analysis, revealing that PEDOT_0.15_C_D had very similar ratio with HA 1.68, followed by PEDOT_0.15_D with a ratio of 1.26 (Fig. 16A).

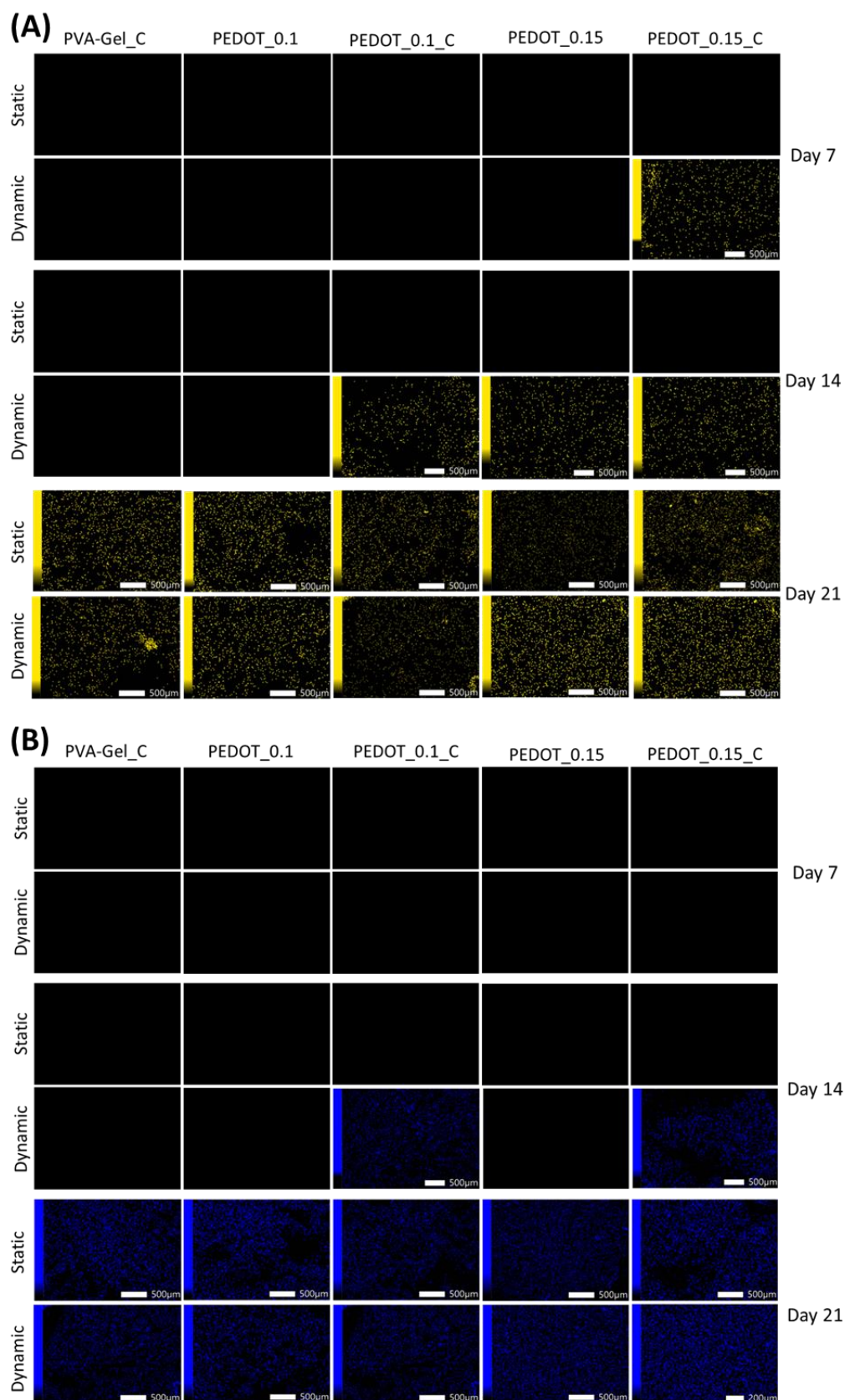


Figure 15. Determination of the calcium and phosphorous mineralization through atomic-resolution mapping and EDS analysis. Calcium is shown in yellow (A) and phosphorous in blue dots (B).

3.3.7. X-ray diffraction (XRD) analysis of biomineralization

For the determination of crystalline structure of the scaffold, XRD analysis was conducted (Fig. 16B). For each sample a corresponding SEM image was obtained in order to visualize the formatted crystals structures (Data not shown). The results of the XRD analysis revealed the presence of prominent peaks corresponding to potential formation of biomineralized matrix. Specifically, PEDOT_0.15_C_D and PEDOT_0.15_D were removed from culture at day 21 and further investigated through XRD analysis. PVA-Gel_C was included as control scaffold. The scaffolds that were chosen were the ones with the most promising EDS results. Their Ca/P ratios align closely with the values of calcium phosphate derivatives and pure HA, suggesting the likelihood of biomineralization due to osteogenesis. PVA-Gel_C_D does not seem to have any sharp peaks, except a small one at approximately 31° 2 θ angle. Moreover, the shape of the crystals match with that of calcium phosphate. For PEDOT_0.15_D, the most prominent peaks are being observed at approximately 31°, 40°, and 46° 2 θ angles. These peaks in combination with the respective Ca/P ratio (Fig. 16A) can be translated as potential formation of calcium phosphate derivatives such as amorphous calcium phosphate (ACP) or octacalcium phosphate (OCP). Ca/P ratios of ACP and OCP range between 1.2 and 1.33 respectively [52] [53] [54] and crystal structure resembles aligned rods in a cohesive arrangement [55], similar with the results for PEDOT_0.15_D. The production of those derivatives is highlighting the ongoing biomineralization process by differentiated pre-osteoblasts. PEDOT_0.15_C_D appear to have sharp peaks at around 31°, and 46° 2 θ angles. Those peaks reflect on (211) and (222) crystallographic planes of HA phase respectively, and are used as reference markers for the identification of hydroxyapatite [56, 57]. The comparison of the Ca/P ratio of PEDOT_0.15_C_D with the established Ca/P ratio of HA (1.67) [58] in combination with XRD analysis, significantly strengthen the evidence supporting the hypothesis of HA formation on the scaffold by mature osteoblasts. Overall, the examination underscores the scaffolds' capacity to support differentiation, highlighting their suitability for promoting bone tissue regeneration.

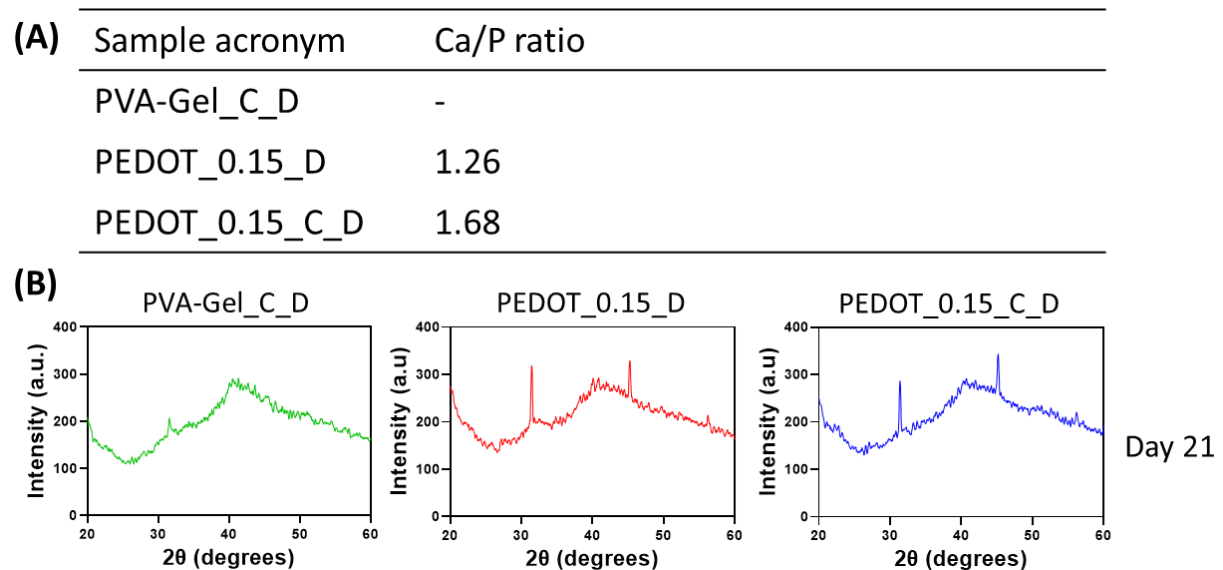


Figure 16. Biomineralization of hydroxyapatite evidenced via Ca/P ratios of the three different scaffolds calculated by EDS analysis (A) and XRD analysis (B). 'S' designates static culture, 'D' dynamic culture (under mechanical stimulation), 'C' crosslinked.

Chapter 4. Discussion

Tissue engineering employs a lot of biomaterials, aiming to engineer cell friendly platforms that support tissue formation. For this purpose, both natural and synthetic biopolymers have been employed, often combined with inorganic components to further reinforce the structural stability and the biological responses. The main objective of this study was the development of a novel scaffold composed of gelatin, a natural polymer, poly(vinyl alcohol) (PVA), a synthetic polymer, and poly(3,4-ethylenedioxythiophene):poly(styrene sulfonate) (PEDOT:PSS), a piezoelectric polymer with potential osteogenic differentiation capabilities. The incorporation of PEDOT:PSS was motivated by its unique ability to convert mechanical stimuli into electrical signals [25], which have been shown to activate voltage-gated calcium channels of the cell membrane [26], a known regulator of osteogenic differentiation [27]. By combining these three components, we aimed to create a multifunctional dynamic scaffold that not only provides structural support and biocompatibility through PVA and gelatin but also harnesses the piezoelectric properties of PEDOT:PSS to potentially enhance osteogenic differentiation under mechanical stimulation.

Mimicking the piezoelectric nature of bone tissue, piezoelectric materials have been found to enhance tissue formation through an electrically active microenvironment without needing an external power source. These materials act as mechanoelectrical transducers, generating an electric field in response to a small mechanical vibration [59]. The grafts incorporating such materials can directly influence the osteoblasts or chondroblasts while improving cell adhesion and proliferation, producing ECM for repairing damaged tissue sites. The mechanotransduction pathway involves mechanoreceptors such as stretch-activated Ca^{2+} channels, cadherins, $\alpha 5\beta 1$ integrin and interleukin-4 (IL-4) loop [60]. Figure 17 depicts the mechanotransduction pathways and other pathway activations in response to electrical and mechanical stimulations. Upon exposure to mechanical stimuli, the piezoelectric smart grafts, due to their molecular asymmetry, are being polarized generating electric signals, that activate the voltage-gated Ca^{2+} channel. An increased intracellular Ca^{2+} concentration further activates calmodulin (calcium-modulated protein), activating the next calcineurin (calcium and calmodulin-dependent serine/threonine protein phosphatase). The activated calcineurin dephosphorylates the NF-AT, causing it to move to the nucleus and act as a transcription factor with other associated proteins[61],[59]. The interaction of intracellular calcium channels and the increase of total Ca^{2+} concentration through connexin, could be one of the mechanisms of osteogenic differentiation of MSCs induced by piezoelectric grafts [62, 63]. Consequently, mechanotransduction pathways could potentially play a pivotal role in bone development and maintenance [25]. The initial hypothesis of the present study was the activation of these mechanotransduction pathways through the mechanical stimulation of PEDOT:PSS-based piezoelectric scaffolds.

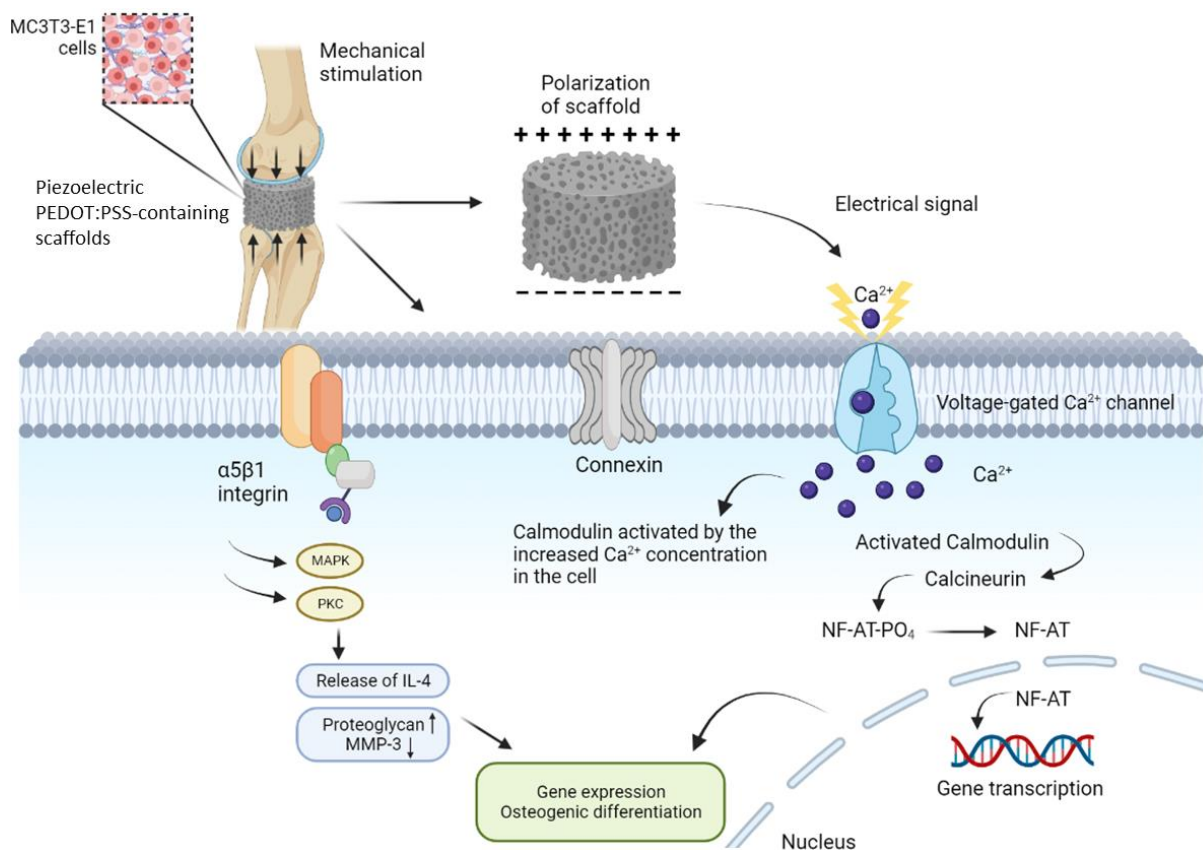


Figure 17. The mechanotransduction pathways involve Ca^{2+} signal-activated pathways and other miscellaneous pathway activation in response to electrical and mechanical stimulation.

To this end, we fabricated and physicochemical characterized PEDOT:PSS-based piezoelectric scaffolds that were then subjected to uniaxial compression by means of MechanoCulture bioreactor. We selected concentrations of 0.1% w/v and 0.15% w/v for the incorporation of PEDOT:PSS into our scaffold fabrication process based on the existing literature and the specific requirements of our study. Prior studies used concentrations from 0.1% w/v to 0.3% PEDOT:PSS [64]. It is well-documented that PEDOT:PSS, when used at concentrations exceeding 0.2%, can exhibit cytotoxic effects on cells [65]. This cytotoxicity poses a significant risk to the viability and health of the cells within our scaffolds, which is a critical concern when developing tissue engineering platforms. Conversely, concentrations below 0.1% w/v have been shown to lack the desired piezoelectric effect on cells, which is a key property we aim to harness for our study. Therefore, the selection of 0.1% w/v and 0.15% w/v PEDOT:PSS concentrations strikes a balance between avoiding cytotoxicity and ensuring the effective promotion of piezoelectric interactions with cells, making them ideal for our scaffold fabrication. By incorporating both concentrations, we aimed to gain deeper insights into the precise dosage required to optimize osteogenesis, ensuring that our scaffold design is not only cytocompatible but also maximally effective in promoting bone tissue formation.

Biological evaluation of the cell proliferation and osteogenic potential of pre-osteoblastic cells, which were loaded onto them, was conducted. The dynamic conditions were selected based on a previous study, using 1 Hz frequency, a cyclic strain of 10% for a duration of 1 h every second day [36], which resemble the physiological applied forces during human body movement [28]. Scaffolds were exposed to mechanical stimulation on their side, mimicking the direction of mechanical forces applied to bone and assuring that the cells cultured within the scaffolds experienced significant levels of strain during mechanical stimulation. Two different concentrations of PEDOT:PSS-containing scaffolds were produced. PVA-Gel_C control scaffolds were mainly employed to determine whether the lack of PEDOT:PSS affect the osteogenic differentiation potential of pre-osteoblasts. Glutaraldehyde was used as crosslinkers to covalently bind the free amino groups of gelatin with the hydroxyl groups of PVA

forming a matrix. GOPS was employed to bind PEDOT:PSS with the rest of the matrix. As it is evident from the biological evaluation, the 2% v/v GOPS and the 0.025% v/v glutaraldehyde did not negatively affect the cell growth and differentiation potential. Similar concentrations of the those crosslinkers have been reported in literature [17, 32] Lyophilization was utilized in the fabrication of the scaffolds, enabling the formation of both larger and smaller pores through the process of water sublimation. This resulted in the 3D structures possessing a favorable setting for supplying nutrients, facilitating cell infiltration, and promoting growth. Moreover, lyophilization served the purpose of an additional crosslinking method, inducing notable enhancements in the flexibility and porosity of the scaffolds.

The FTIR spectra provide the information of the hydrogel formation from the initiators as well as the crosslinking [66]. FTIR was performed to check for successful bonding of PEDOT:PSS with the PVA-Gelatin matrix, as well as successful attachment of the GOPS and glutaraldehyde molecules. The peak correlating with the formation of the C=C in PEDOT is seen at about 1510 cm^{-1} indicating the successful attachment of GOPS to the interpenetrating polymer network of PEDOT:PSS [67]. As for the possible crosslinking reaction mechanism between PEDOT:PSS and GOPS, it is reported in the literature that the SO_3^- groups of the excess PSS reacts with the epoxy ring of GOPS [68] The FTIR spectra analysis of the scaffolds depicted similar characteristic peaks with those of their base constituents. These characteristic peaks were consistent across all PEDOT:PSS-containing scaffolds, confirming successful integration. Crosslinked scaffolds displayed a prominent peak, indicating effective crosslinking between the matrix and PEDOT:PSS. Conversely, non-crosslinked scaffolds showed weaker binding of PEDOT:PSS. Control scaffolds demonstrated stability and interactions between Gelatin's positive charges [47] and PVA's negative charges [48]. In the case of gelatin, the glutaraldehyde reacts with each NH_2 functional group of adjacent lysine residues, while for PVA the glutaraldehyde reacts with two adjacent hydroxyl groups, forming acetal bridges [69].

The degradation rates of different scaffold compositions were evaluated at intervals of 4, 7, 14, 21, and 28 days. PVA_Gel scaffolds demonstrated the highest degradation rates, which can be ascribed to the fact that the gelatin component, in incubation conditions, exists in a liquid state. Consequently, during the degradation experiment at 37°C in the incubator, the gelatin part of the scaffolds dissolved. Furthermore, the level of crosslinking appears to be insufficient, as a similar pattern is observed in the case of PVA_Gel_C scaffolds. On the other hand, PEDOT:PSS-containing scaffolds appear to have significantly lower degradation rates. This could be attributed to the presence of the conductive polymer PEDOT:PSS. According to existing literature, when subjected to freezing-thawing cycles, PEDOT:PSS undergoes reshaping. This means that structural alternations or changes within the PEDOT:PSS polymer could occur. These changes can involve the rearrangement of the molecular structure and the formation of new bonds, which contribute to improved integrity over time and enhanced mechanical properties [31]. Generally, PEDOT:PSS-containing scaffolds retained initial weight and integrity over 21 days in culture without noticeable swelling or morphological changes, which holds particular significance for load-bearing areas like human cartilage, where mechanical resilience during the healing process is vital [49].

Swelling behavior affects the scaffolds' 3D structure and mechanical strength. When scaffolds swell, their pore size increase, which can enhance cell attachment and migration but can adversely affect their mechanical properties [70]. Both crosslinked and non-crosslinked scaffolds showed swelling capability. PEDOT_0.15_C demonstrated improved absorption compared to PEDOT_0.15. Significant differences were observed between PEDOT_0.15_C and its control PVA-Gel_C, as well as PEDOT_0.15 and PVA-Gel

Natural bone has internal pores, known as voids, with their volume referred to as porosity. Porous scaffolds facilitate cell penetration and migration [71]. Porosity determines permeability, allowing for nutrient and oxygen exchange, waste removal, and the ingrowth of bone tissue and blood vessels [72]. Smaller pores can limit vascular invasion, favoring chondrogenesis, while larger pores can promote osteogenesis due to higher oxygen levels [73]. Porosity of the scaffolds was illustrated using SEM images and quantified through both the liquid displacement method using ethanol and SEM

images analyzed with ImageJ. Notably, PEDOT:PSS-containing scaffolds exhibited elevated porosity compared to control scaffolds. Specifically, PEDOT_0.15_C showcased the highest porosity as well as the most well-defined pores, surpassing PEDOT_0.15 with fewer and more elongated pores. This trend extended to PEDOT_0.1 scaffolds, with the crosslinked variant slightly exceeding the non-crosslinked. The PVA-Gel control scaffold exhibited the lowest porosity. In general, the porosity of our scaffolds does not exceed 60%, which differs from the typical porosity levels reported in the literature, usually falling within the range of 80-85% for gelatin containing scaffolds [34, 35]. This variance can be attributed to the elevated PVA concentration within the scaffolds, resulting in increased rigidity. As previous studies have shown, higher PVA concentrations tend to reduce porosity [74]. In our research, 5% PVA concentration was chosen, which yielded a scaffold porosity of 60%. However, our choice of using this specific PVA percentage was driven by the exceptional mechanical properties it imparts to the scaffolds. This aspect is of utmost importance for the primary goal of our study, which is to subject the scaffolds to mechanical stimulation. Therefore, our aim was to develop scaffolds with high elasticity to withstand the mechanical loads applied to them.

The electrical conductivity of the three different compositions was evaluated. It is noteworthy that the addition of PEDOT:PSS led to a substantial increase in the electrical conductivity when compared to the control, aligning with the existing literature suggesting that increasing PEDOT:PSS concentration within a specific range, results in heightened electrical conductivity levels [64, 65]. The comparative analysis between PEDOT_0.1 and PEDOT_0.15 samples did not reveal any statistically significant differences in conductivity. However, it is intriguing to observe that PEDOT_0.15 exhibited the highest values among the tested samples, underscoring its potential to enhance the scaffolds conductivity.

In the context of mechanical characterization, PEDOT_0.15_C scaffold exhibited superior elasticity compared to the PVA-Gel_C control scaffold, while PEDOT_0.1_C closely mirrored the control. Similarly, non-crosslinked scaffolds, PEDOT_0.1 and PEDOT_0.15, displayed notably higher moduli than the PVA-Gel control scaffold. Previous studies have indicated that PVA/Gelatin hydrogels typically exhibit a Young modulus of approximately 40-300 kPa [24, 75, 76]. In the present study, PEDOT:PSS/PVA/Gelatin scaffolds exceeded the reported values. Scaffolds fully recovered to their initial height after the compression test, without any visible damage. This exceptional performance holds significant promise for their application in bone tissue engineering.

Overall, the physicochemical analysis of the scaffolds underscores the pivotal role of crosslinking in enhancing scaffold integrity and promoting material interactions. These findings, coupled with the notably high Young's modulus values, shed light on the profound impact of PEDOT:PSS incorporation and crosslinking on scaffold rigidity, offering promising prospects for their utilization in tissue engineering endeavors. Moreover, the controlled degradation exhibited by PEDOT:PSS-enhanced scaffolds, along with their favorable swelling ratios, highlights their potential to withstand the mechanical demands of tissue regeneration. Additionally, the elevated porosity observed in PEDOT:PSS-containing scaffolds further accentuates the advantages of PEDOT:PSS integration, facilitating cellular infiltration, nutrient transport, and seamless tissue integration. Collectively, these results endorse the potential of these scaffolds as versatile and robust platforms for advancing various tissue engineering applications.

PEDOT:PSS-containing hydrogels show optimal cell adhesion and elongation while control scaffolds have linear proliferation. Networks of interconnected cells seem to have been formatted. Cell viability and proliferation demonstrate increasing cell numbers in all hydrogel types. Day 3 shows significant growth compared to the control, especially in PEDOT_0.15 at day 7. The increase of PEDOT:PSS concentration proves to have an important effect on the cell number, which is in line with other reports on cell viability of PEDOT:PSS-containing scaffolds [17, 29].

Early healing phase is particularly sensitive to mechanical signals and lay the foundations for the entire repair process. In fact, it has been shown that allowing limited interfragmentary movement

in the initial phase can enhance fracture healing in sheep models [77]. The movement of the impact fracture of axial fracture is reported as the main loading system for animal bone marrow models with an external fixator [78]. The compression of axial fracture that occurs as a result of weight bearing in experimental bone healing studies is between 10% and 33% [79, 80] and 2% and 20% respectively [81, 82], in the fracture gaps for sheep and rat bone marrow. According to reported *in vivo* data and to previous studies investigating the effects of mechanical loading on cell differentiation, 5 and 10% of strain regimes were chosen [83-86]. In order to mimic the load pattern in human movement, sinusoidal compression at 1 Hz frequency was applied by means of a bioreactor. Overall, the load parameters used in this study are selected to represent the mechanical environment in the early fracture gap, more specifically the dynamic environment that occurs *in vivo*.

The morphology as well as the osteogenic differentiation potential of pre-osteoblasts seeded on the scaffolds, during the mechanical stimulation experiment, were examined. SEM images display the morphology of pre-osteoblasts onto the scaffolds and highlight strong cell adhesion, characterized by elongated morphology and increasing proliferation up to day 14. Notably, dynamic conditions foster substantial cell proliferation and adhesion by day 7 across all scaffold types. PEDOT_0.15_D and PEDOT_0.15_C_D exhibit well-spread cells, some with pseudopodia by day 7. By day 14, cells display heightened adhesion and cytoskeletal organization on the biomaterial, indicating a favorable response. The extensive cell coverage on scaffold surfaces, forming dense cell sheets of fully spread pre-osteoblasts, underscores exceptional scaffold biocompatibility and capacity to support cell growth and interaction.

ALP is an enzyme that is widely distributed in different tissues and is particularly associated with bone formation, where it is involved in mineralization processes. The main role of this enzyme is to detach phosphate groups off different molecules and consequently inducing the formation of HA crystals, a fundamental component of extracellular matrix of bone tissue [87]. Alkaline phosphatase (ALP), was assessed through live staining and confocal microscopy. PEDOT_0.15_C_D exhibits higher ALP activity at day 3, followed by PEDOT_0.1_C_D, a trend continuing with less intensity in the following time points, due to ALP's early marker nature. Dynamic conditions consistently outperform static ones. The incorporation of PEDOT:PSS into the PVA/Gelatin matrix emerges as pivotal for osteogenic differentiation, particularly in crosslinked scaffolds that successfully integrate PEDOT:PSS, showcasing its piezoelectric influence triggering osteogenic differentiation. The above findings are in line with the existing literature, which supports that PEDOT:PSS serves as a osteogenic differentiation stimulus for the pre-osteoblastic cells [17] [88].

Calcium deposition, a bone formation indicator, is more pronounced under mechanical stimulation, especially in PEDOT_0.15_D, PEDOT_0.15_C_D, and PEDOT_0.1_D. Collagen type I, a structural bone tissue component, displays steady increase in both dynamic and static cultures. Mechanically stimulated scaffolds maintain higher collagen levels by day 21, especially PEDOT_0.15_C_D.

EDS uncovered significant calcium and phosphorus deposition across diverse scaffolds. Particularly, at day 7, calcium deposition was evident in PEDOT_0.15_C_D, and by day 14, three dynamic culture scaffolds, including PEDOT_0.1_C_D, PEDOT_0.15_D, and PEDOT_0.15_C_D, exhibited calcium deposition, corroborating the previously assessed osteogenic markers and highlighting PEDOT:PSS's osteogenic role. By day 21, calcium deposition was widespread across all scaffolds. Furthermore, phosphorus biomineralization emerged in all scaffolds by day 21, compared to its presence only in PEDOT_0.1_C_D and PEDOT_0.15_C_D at day 14. Similar results are evident in previous studies that show the important role of PEDOT:PSS in biomineralization, [17],[89] a fundamental process for bone tissue formation, potentially involving hydroxyapatite, a major bone component. Ca/P ratios, assessed via EDS analysis, revealed similarities between PEDOT_0.15_C_D and hydroxyapatite, followed by PEDOT_0.15_D. X-ray diffraction (XRD) analysis, identified prominent peaks suggesting biomineralized matrix formation. Particularly, PEDOT_0.15_C_D and PEDOT_0.15_D, exhibited peaks reminiscent of calcium phosphate derivatives. For PEDOT_0.15_C_D, sharp peaks at

characteristic hydroxyapatite angles were identified. This close correlation of, XRD, and Ca/P ratios strongly supports the hydroxyapatite hypothesis. Collectively, this examination accentuates the scaffolds' potential to drive osteogenic differentiation, affirming their suitability for facilitating bone tissue regeneration.

Chapter 5. Conclusion

In summary, our study underscores the pivotal role of mechanically sensitive scaffolds in advancing osteogenic tissue regeneration. The outcomes of this investigation spotlight the significant potential of the PEDOT:PSS/PVA/Gelatin scaffolds, which intricately support pre-osteoblast adhesion, proliferation, and osteogenic differentiation under simulated mechanical stimulation akin to the natural dynamics of bone tissue. Notably, scaffolds featuring the PEDOT_0.15_C composition, under mechanical stimulation conditions, exhibited statistically remarkable enhancement in osteogenic differentiation, evident through the detection of hydroxyapatite on scaffolds after 21 days. These scaffolds hold promise for applications in bone tissue engineering and other mechanically-loaded tissues. Furthermore, our pioneering development of a holistic 3D tension-controlled scaffold model, combined with dynamic culture of pre-osteoblasts, establishes an innovative platform for studying osteogenesis under conditions closely resembling the body's natural state. This approach not only contributes to advancing *in vitro* evaluation methods but also significantly reduces the need for *in vivo* experimentation. Moreover, our findings validate our initial hypothesis regarding the activation of mechanotransduction pathways through the mechanical stimulation of PEDOT:PSS-based piezoelectric scaffolds. This not only positions these smart biomaterials as potential future bone implants but also underscores their role as a comprehensive model for observing and studying osteogenesis in depth.

References

- [1] M. Alonzo, F. Alvarez Primo, S. Anil Kumar, J.A. Mudloff, E. Dominguez, G. Fregoso, N. Ortiz, W.M. Weiss, B. Joddar, Bone tissue engineering techniques, advances, and scaffolds for treatment of bone defects, *Current Opinion in Biomedical Engineering* 17 (2021) 100248.
- [2] G.L. Koons, M. Diba, A.G. Mikos, Materials design for bone-tissue engineering, *Nature Reviews Materials* 5(8) (2020) 584-603.
- [3] S. Bose, M. Roy, A. Bandyopadhyay, Recent advances in bone tissue engineering scaffolds, *Trends in biotechnology* 30(10) (2012) 546-54.
- [4] S. Bose, M. Roy, A. Bandyopadhyay, Recent advances in bone tissue engineering scaffolds, *Trends in Biotechnology* 30(10) (2012) 546-554.
- [5] K. Joyce, G.T. Fabra, Y. Bozkurt, A. Pandit, Bioactive potential of natural biomaterials: identification, retention and assessment of biological properties, *Signal Transduction and Targeted Therapy* 6(1) (2021) 122.
- [6] H. Qu, H. Fu, Z. Han, Y. Sun, Biomaterials for bone tissue engineering scaffolds: a review, *RSC Advances* 9(45) (2019) 26252-26262.
- [7] M.N. Collins, G. Ren, K. Young, S. Pina, R.L. Reis, J.M. Oliveira, Scaffold Fabrication Technologies and Structure/Function Properties in Bone Tissue Engineering, *Advanced Functional Materials* 31(21) (2021) 2010609.
- [8] R.S. Valtanen, Y.P. Yang, G.C. Gurtner, W.J. Maloney, D.W. Lowenberg, Synthetic and Bone tissue engineering graft substitutes: What is the future?, *Injury* 52 (2021) S72-S77.
- [9] F.R. Maia, A.R. Bastos, J.M. Oliveira, V.M. Correlo, R.L. Reis, Recent approaches towards bone tissue engineering, *Bone* 154 (2022) 116256.
- [10] H. Wei, J. Cui, K. Lin, J. Xie, X. Wang, Recent advances in smart stimuli-responsive biomaterials for bone therapeutics and regeneration, *Bone Research* 10(1) (2022) 17.
- [11] H.M. El-Husseiny, E.A. Mady, W.A. El-Dakroury, M.B. Zewail, M. Noshay, A.M. Abdelfatah, A.S. Doghish, Smart/stimuli-responsive hydrogels: State-of-the-art platforms for bone tissue engineering, *Applied Materials Today* 29 (2022) 101560.
- [12] A. Samadi, M.A. Salati, A. Safari, M. Jouyandeh, M. Barani, N.P. Singh Chauhan, E.G. Golab, P. Zarrintaj, S. Kar, F. Seidi, A. Hejna, M.R. Saeb, Comparative review of piezoelectric biomaterials approach for bone tissue engineering, *Journal of Biomaterials Science, Polymer Edition* 33(12) (2022) 1555-1594.
- [13] V. Jarkov, S.J. Allan, C. Bowen, H. Khanbareh, Piezoelectric materials and systems for tissue engineering and implantable energy harvesting devices for biomedical applications, *International Materials Reviews* 67(7) (2022) 683-733.
- [14] B.P. Hung, D.L. Hutton, W.L. Grayson, Mechanical control of tissue-engineered bone, *Stem Cell Research & Therapy* 4(1) (2013) 10.
- [15] H.M. El-Husseiny, E.A. Mady, L. Hamabe, A. Abugomaa, K. Shimada, T. Yoshida, T. Tanaka, A. Yokoi, M. Elbadawy, R. Tanaka, Smart/stimuli-responsive hydrogels: Cutting-edge platforms for tissue engineering and other biomedical applications, *Materials Today Bio* 13 (2022) 100186.
- [16] R. Florencio-Silva, G.R. Sasso, E. Sasso-Cerri, M.J. Simões, P.S. Cerri, Biology of Bone Tissue: Structure, Function, and Factors That Influence Bone Cells, *BioMed research international* 2015 (2015) 421746.
- [17] A.G. Guex, J.L. Puetzer, A. Armgarth, E. Littmann, E. Stavrinidou, E.P. Giannelis, G.G. Malliaras, M.M. Stevens, Highly porous scaffolds of PEDOT:PSS for bone tissue engineering, *Acta biomaterialia* 62 (2017) 91-101.
- [18] Y.-F. Zhang, M.-M. Guo, Y. Zhang, C.Y. Tang, C. Jiang, Y. Dong, W.-C. Law, F.-P. Du, Flexible, stretchable and conductive PVA/PEDOT:PSS composite hydrogels prepared by SIPN strategy, *Polymer Testing* 81 (2020) 106213.
- [19] F. Ghorbani, B. Ghalandari, M. Sahranavard, A. Zamanian, M.N. Collins, Tuning the biomimetic behavior of hybrid scaffolds for bone tissue engineering through surface modifications and drug immobilization, *Materials Science and Engineering: C* 130 (2021) 112434.

- [20] K. Hayashi, Y. Tabata, Preparation of stem cell aggregates with gelatin microspheres to enhance biological functions, *Acta biomaterialia* 7(7) (2011) 2797-2803.
- [21] I. Lukin, I. Erezuma, L. Maeso, J. Zarate, M.F. Desimone, Progress in Gelatin as Biomaterial for Tissue Engineering, 14(6) (2022).
- [22] A. Thomas, J. Bera, Preparation and characterization of gelatin-bioactive glass ceramic scaffolds for bone tissue engineering, *Journal of Biomaterials Science, Polymer Edition* 30(7) (2019) 561-579.
- [23] A. Kumar, S.S. Han, PVA-based hydrogels for tissue engineering: A review, *International Journal of Polymeric Materials and Polymeric Biomaterials* 66(4) (2017) 159-182.
- [24] A. Thangprasert, C. Tansakul, N. Thuaksubun, J. Meesane, Mimicked hybrid hydrogel based on gelatin/PVA for tissue engineering in subchondral bone interface for osteoarthritis surgery, *Materials & Design* 183 (2019) 108113.
- [25] D. D'Alessandro, C. Ricci, M. Milazzo, G. Strangis, F. Forli, G. Buda, M. Petrini, S. Berrettini, M.J. Uddin, S. Danti, P. Parchi, Piezoelectric Signals in Vascularized Bone Regeneration, *Biomolecules* 11(11) (2021).
- [26] D. Lee, H. Zhang, S. Ryu, Elastic Modulus Measurement of Hydrogels, in: M.I.H. Mondal (Ed.), *Cellulose-Based Superabsorbent Hydrogels*, Springer International Publishing, Cham, 2018, pp. 1-21.
- [27] Y.Z. Tan, D.D. Fei, X.N. He, J.M. Dai, R.C. Xu, X.Y. Xu, J.J. Wu, B. Li, L-type voltage-gated calcium channels in stem cells and tissue engineering, *Cell proliferation* 52(4) (2019) e12623.
- [28] S. Schreivogel, V. Kuchibhotla, P. Knaus, G.N. Duda, A. Petersen, Load-induced osteogenic differentiation of mesenchymal stromal cells is caused by mechano-regulated autocrine signaling, *Journal of tissue engineering and regenerative medicine* 13(11) (2019) 1992-2008.
- [29] F. Furlani, E. Campodoni, N. Sangiorgi, M. Montesi, A. Sanson, M. Sandri, S. Panseri, Electroconductive scaffolds based on gelatin and PEDOT:PSS for cardiac regeneration, *International Journal of Biological Macromolecules* 224 (2023) 266-280.
- [30] P.M. Gotovtsev, G.U. Badranova, Y.V. Zubavichus, N.K. Chumakov, C.G. Antipova, R.A. Kamyshinsky, M.Y. Presniakov, K.V. Tokaev, T.E. Grigoriev, Electroconductive PEDOT:PSS-based hydrogel prepared by freezing-thawing method, *Heliyon* 5(9) (2019) e02498.
- [31] W. Li, H. Lu, N. Zhang, M. Ma, Enhancing the Properties of Conductive Polymer Hydrogels by Freeze–Thaw Cycles for High-Performance Flexible Supercapacitors, *ACS Applied Materials & Interfaces* 9(23) (2017) 20142-20149.
- [32] A.P. McGuigan, M.V. Sefton, Modular tissue engineering: fabrication of a gelatin-based construct, 1(2) (2007) 136-145.
- [33] F.K. Metze, S. Sant, Z. Meng, H.-A. Klok, K. Kaur, Swelling-Activated, Soft Mechanochemistry in Polymer Materials, *Langmuir* 39(10) (2023) 3546-3557.
- [34] K. Loukelis, D. Papadogianni, M. Chatzinikolaïdou, Kappa-carrageenan/chitosan/gelatin scaffolds enriched with potassium chloride for bone tissue engineering, *International Journal of Biological Macromolecules* 209 (2022) 1720-1730.
- [35] A. Georgopoulou, F. Papadogiannis, A. Batsali, J. Marakis, K. Alpantaki, A.G. Eliopoulos, C. Pontikoglou, M. Chatzinikolaïdou, Chitosan/gelatin scaffolds support bone regeneration, *Journal of materials science. Materials in medicine* 29(5) (2018) 59.
- [36] G.-I. Kontogianni, K. Loukelis, A.F. Bonatti, E. Batoni, C. De Maria, R. Naseem, K. Dalgarno, G. Vozzi, D.B. MacManus, S. Mondal, N. Dunne, C. Vitale-Brovarone, M. Chatzinikolaïdou, Effect of Uniaxial Compression Frequency on Osteogenic Cell Responses in Dynamic 3D Cultures, 10(5) (2023) 532.
- [37] U. Singh, R.H. Quintanilla, S. Grecian, K.R. Gee, M.S. Rao, U. Lakshmipathy, Novel Live Alkaline Phosphatase Substrate for Identification of Pluripotent Stem Cells, *Stem Cell Reviews and Reports* 8(3) (2012) 1021-1029.
- [38] N.S. Fedarko, Chapter 5 - Osteoblast/Osteoclast Development and Function in Osteogenesis Imperfecta, in: J.R. Shapiro, P.H. Byers, F.H. Glorieux, P.D. Sponseller (Eds.), *Osteogenesis Imperfecta*, Academic Press, San Diego, 2014, pp. 45-56.
- [39] F.J. Geissel, V. Platania, N. DeBerardinis, C. Skjöldebrand, G.N. Belibasakis, C. Persson, G. Hulsart-Billström, M. Chatzinikolaïdou, G.A. Sotiriou, Nanostructured Ag-Bioglass Implant Coatings with Antibacterial and Osteogenic Activity, 10(3) (2023) 2201980.

- [40] L. Rittié, Method for Picrosirius Red-Polarization Detection of Collagen Fibers in Tissue Sections, *Methods in molecular biology* (Clifton, N.J.) 1627 (2017) 395-407.
- [41] K. Petropoulou, V. Platania, M. Chatzinikolaidou, A. Mitraki, A Doubly Fmoc-Protected Aspartic Acid Self-Assembles into Hydrogels Suitable for Bone Tissue Engineering, 15(24) (2022) 8928.
- [42] M.A. El-Meligy, K. Valachová, I. Juránek, T.M. Tamer, L. Šoltés, Preparation and Physicochemical Characterization of Gelatin-Aldehyde Derivatives, *Molecules* (Basel, Switzerland) 27(20) (2022).
- [43] H. Hu, J.H. Xin, H. Hu, A. Chan, L. He, Glutaraldehyde–chitosan and poly (vinyl alcohol) blends, and fluorescence of their nano-silica composite films, *Carbohydrate Polymers* 91(1) (2013) 305-313.
- [44] N.M. Sadiq, S.B. Aziz, M.F.Z. Kadir, Development of Flexible Plasticized Ion Conducting Polymer Blend Electrolytes Based on Polyvinyl Alcohol (PVA): Chitosan (CS) with High Ion Transport Parameters Close to Gel Based Electrolytes, 8(3) (2022) 153.
- [45] N. Kanjana, W. Maiaugree, P. Laokul, I. Chaiya, T. Lunnoo, P. Wongjom, Y. Infahsaeng, B. Thongdang, V. Amornkitbamrung, Fly ash boosted electrocatalytic properties of PEDOT:PSS counter electrodes for the triiodide reduction in dye-sensitized solar cells, *Scientific Reports* 13(1) (2023) 6012.
- [46] Ö. Yağci, O.K. Özdemir, Improving the electrical conductivity and electrochemical properties of PEDOT:PSS thin films by Ca and Mg doping, *Polymer Bulletin* 79(12) (2022) 11493-11509.
- [47] F. Alihosseini, 10 - Plant-based compounds for antimicrobial textiles, in: G. Sun (Ed.), *Antimicrobial Textiles*, Woodhead Publishing 2016, pp. 155-195.
- [48] M. Wiśniewska, V. Bogatyrov, I. Ostolska, K. Szewczuk-Karpisz, K. Terpiłowski, A. Nosal-Wiercińska, Impact of poly(vinyl alcohol) adsorption on the surface characteristics of mixed oxide $Mn_xO_y-SiO_2$, *Adsorption* 22(4) (2016) 417-423.
- [49] T. Winkler, F.A. Sass, G.N. Duda, K. Schmidt-Bleek, A review of biomaterials in bone defect healing, remaining shortcomings and future opportunities for bone tissue engineering: The unsolved challenge, *Bone & joint research* 7(3) (2018) 232-243.
- [50] Y. Tanikake, M. Akahane, A. Furukawa, Y. Tohma, Y. Inagaki, T. Kira, Y. Tanaka, Calcium Concentration in Culture Medium as a Nondestructive and Rapid Marker of Osteogenesis, 26(6) (2017) 1067-1076.
- [51] M. Salehi, V. Leung-Pineda, Chapter 12 - Disorders of calcium and phosphate metabolism in infants and children, in: D. Dietzen, M. Bennett, E. Wong, S. Haymond (Eds.), *Biochemical and Molecular Basis of Pediatric Disease* (Fifth Edition), Academic Press 2021, pp. 379-410.
- [52] P. Habibovic, J. Li, C.M. van der Valk, G. Meijer, P. Layrolle, C.A. van Blitterswijk, K. de Groot, Biological performance of uncoated and octacalcium phosphate-coated Ti6Al4V, *Biomaterials* 26(1) (2005) 23-36.
- [53] M. Szekeres, G. Fodor, A. Fazekas, M. Radnai, K. Turzó, I. Dékány, Formation of octacalcium phosphate by heterogeneous nucleation on a titania surface, *Colloid and Polymer Science* 283(6) (2005) 587-592.
- [54] T. Yokoi, M. Shimabukuro, M. Kawashita, Octacalcium phosphate with incorporated carboxylate ions: a review, *Science and Technology of Advanced Materials* 23(1) (2022) 434-445.
- [55] N.V. Petrakova, A.Y. Teterina, P.V. Mikheeva, S.A. Akhmedova, E.A. Kuvshinova, I.K. Sviridova, N.S. Sergeeva, I.V. Smirnov, A.Y. Fedotov, Y.F. Kargin, S.M. Barinov, V.S. Komlev, In Vitro Study of Octacalcium Phosphate Behavior in Different Model Solutions, *ACS Omega* 6(11) (2021) 7487-7498.
- [56] E. Tian, F. Watanabe, B. Martin, M. Zangari, Innate Biomineralization, 21(14) (2020) 4820.
- [57] J.O. Akindoyo, S. Ghazali, M.D.H. Beg, N. Jeyaratnam, Characterization and Elemental Quantification of Natural Hydroxyapatite Produced from Cow Bone, 42(9) (2019) 1805-1815.
- [58] J. Jeong, J.H. Kim, J.H. Shim, N.S. Hwang, C.Y. Heo, Bioactive calcium phosphate materials and applications in bone regeneration, *Biomaterials Research* 23(1) (2019) 4.
- [59] J. Jacob, N. More, K. Kalia, G. Kapusetti, Piezoelectric smart biomaterials for bone and cartilage tissue engineering, *Inflammation and Regeneration* 38(1) (2018) 2.
- [60] H.S. Lee, S.J. Millward-Sadler, M.O. Wright, G. Nuki, R. Al-Jamal, D.M. Salter, Activation of Integrin—RACK1/PKC α signalling in human articular chondrocyte mechanotransduction, *Osteoarthritis and Cartilage* 10(11) (2002) 890-897.

- [61] T. Kanno, T. Takahashi, T. Tsujisawa, W. Ariyoshi, T. Nishihara, Mechanical stress-mediated Runx2 activation is dependent on Ras/ERK1/2 MAPK signaling in osteoblasts, *Journal of cellular biochemistry* 101(5) (2007) 1266-77.
- [62] M. Kitsara, A. Blanquer, G. Murillo, V. Humblot, S. De Bragança Vieira, C. Nogués, E. Ibáñez, J. Esteve, L. Barrios, Permanently hydrophilic, piezoelectric PVDF nanofibrous scaffolds promoting unaided electromechanical stimulation on osteoblasts, *Nanoscale* 11(18) (2019) 8906-8917.
- [63] X. Zhang, L. Li, J. Ouyang, L. Zhang, J. Xue, H. Zhang, W. Tao, Electroactive electrospun nanofibers for tissue engineering, *Nano Today* 39 (2021) 101196.
- [64] A. Shahini, M. Yazdimamaghani, K.J. Walker, M.A. Eastman, H. Hatami-Marbini, B.J. Smith, J.L. Ricci, S.V. Madhally, D. Vashaee, L. Tayebi, 3D conductive nanocomposite scaffold for bone tissue engineering, *Int J Nanomedicine* 9 (2014) 167-81.
- [65] P. Bhattacharjee, M. Ahearne, Fabrication and Biocompatibility of Electroconductive Silk Fibroin/PEDOT: PSS Composites for Corneal Epithelial Regeneration, 12(12) (2020) 3028.
- [66] M. Thürmer, C. Diehl, F. Bento Brum, L.A. Dos Santos, Preparation and Characterization of Hydrogels with Potential for Use as Biomaterials, *Materials Research* 17 (2014) 109-113.
- [67] P.M. Smith, I. Sutradhar, M. Telmer, R. Magar, A.B. Farimani, B. Reeja-Jayan, Isolating Specific vs. Non-Specific Binding Responses in Conducting Polymer Biosensors for Bio-Fingerprinting, 21(19) (2021) 6335.
- [68] A. Håkansson, S. Han, S. Wang, J. Lu, S. Braun, M. Fahlman, M. Berggren, X. Crispin, S. Fabiano, Effect of (3-glycidyloxypropyl)trimethoxysilane (GOPS) on the electrical properties of PEDOT:PSS films, 55(10) (2017) 814-820.
- [69] P.M.A. Alves, R.A. Carvalho, I.C.F. Moraes, C.G. Luciano, A.M.Q.B. Bittante, P.J.A. Sobral, Development of films based on blends of gelatin and poly(vinyl alcohol) cross linked with glutaraldehyde, *Food Hydrocolloids* 25(7) (2011) 1751-1757.
- [70] C. Shi, X. Hou, D. Zhao, H. Wang, R. Guo, Y. Zhou, Preparation of the bioglass/chitosan-alginate composite scaffolds with high bioactivity and mechanical properties as bone graft materials, *Journal of the Mechanical Behavior of Biomedical Materials* 126 (2022) 105062.
- [71] W. Bonfield, Designing porous scaffolds for tissue engineering, 364(1838) (2006) 227-232.
- [72] A. Teimouri, S. Roohafza, M. Azadi, A.N. Chermahini, Fabrication and characterization of chitosan/gelatin/nanodiopside composite scaffolds for tissue engineering application, *Polymer Bulletin* 75(4) (2018) 1487-1504.
- [73] M.I. Santos, R.L. Reis, Vascularization in Bone Tissue Engineering: Physiology, Current Strategies, Major Hurdles and Future Challenges, 10(1) (2010) 12-27.
- [74] Hartatiek, Yudyanto, M.I. Wuriatika, J. Utomo, M. Nurhuda, Masrurroh, D.J.D.H. Santjojo, Nanostructure, porosity and tensile strength of PVA/Hydroxyapatite composite nanofiber for bone tissue engineering, *Materials Today: Proceedings* 44 (2021) 3203-3206.
- [75] H. Kim, G.H. Yang, G. Kim, Three-dimensional gelatin/PVA scaffold with nanofibrillated collagen surface for applications in hard-tissue regeneration, *International Journal of Biological Macromolecules* 135 (2019) 21-28.
- [76] H. Kim, G.H. Yang, C.H. Choi, Y.S. Cho, G. Kim, Gelatin/PVA scaffolds fabricated using a 3D-printing process employed with a low-temperature plate for hard tissue regeneration: Fabrication and characterizations, *International Journal of Biological Macromolecules* 120 (2018) 119-127.
- [77] P. Klein, H. Schell, F. Streitparth, M. Heller, J.P. Kassi, F. Kandziora, H. Bragulla, N.P. Haas, G.N. Duda, The initial phase of fracture healing is specifically sensitive to mechanical conditions, *Journal of orthopaedic research : official publication of the Orthopaedic Research Society* 21(4) (2003) 662-9.
- [78] M. Bottlang, F. Feist, Biomechanics of far cortical locking, *Journal of orthopaedic trauma* 25 Suppl 1(Suppl 1) (2011) S21-8.
- [79] J. Klein-Nulend, J. Roelofsen, C.M. Semeins, A.L. Bronckers, E.H. Burger, Mechanical stimulation of osteopontin mRNA expression and synthesis in bone cell cultures, *Journal of cellular physiology* 170(2) (1997) 174-81.

- [80] H. Schell, M.S. Thompson, H.J. Bail, J.E. Hoffmann, A. Schill, G.N. Duda, J. Lienau, Mechanical induction of critically delayed bone healing in sheep: radiological and biomechanical results, *Journal of biomechanics* 41(14) (2008) 3066-72.
- [81] L.E. Claes, C.A. Heigele, Magnitudes of local stress and strain along bony surfaces predict the course and type of fracture healing, *Journal of biomechanics* 32(3) (1999) 255-66.
- [82] B.S. Klosterhoff, K.G. Ong, L. Krishnan, K.M. Hetzendorfer, Y.H. Chang, M.G. Allen, R.E. Guldberg, N.J. Willett, Wireless Implantable Sensor for Noninvasive, Longitudinal Quantification of Axial Strain Across Rodent Long Bone Defects, *JOURNAL OF BIOMECHANICAL ENGINEERING-TRANSACTIONS OF THE ASME* 139(11) (2017).
- [83] M. Jagodzinski, A. Breitbart, M. Wehmeier, E. Hesse, C. Haasper, C. Krettek, J. Zeichen, S. Hankemeier, Influence of perfusion and cyclic compression on proliferation and differentiation of bone marrow stromal cells in 3-dimensional culture, *Journal of biomechanics* 41(9) (2008) 1885-91.
- [84] E. Michalopoulos, R.L. Knight, S. Korossis, J.N. Kearney, J. Fisher, E. Ingham, Development of methods for studying the differentiation of human mesenchymal stem cells under cyclic compressive strain, *Tissue engineering. Part C, Methods* 18(4) (2012) 252-62.
- [85] C. Liu, R. Abedian, R. Meister, C. Haasper, C. Hurschler, C. Krettek, G. von Lewinski, M. Jagodzinski, Influence of perfusion and compression on the proliferation and differentiation of bone mesenchymal stromal cells seeded on polyurethane scaffolds, *Biomaterials* 33(4) (2012) 1052-64.
- [86] A. Sittichokechaiwut, J.H. Edwards, A.M. Scutt, G.C. Reilly, Short bouts of mechanical loading are as effective as dexamethasone at inducing matrix production by human bone marrow mesenchymal stem cell, *European cells & materials* 20 (2010) 45-57.
- [87] S. Vimalraj, Alkaline phosphatase: Structure, expression and its function in bone mineralization, *Gene* 754 (2020) 144855.
- [88] N. Fani, M. Hajinasrollah, M. Asghari Vostikolaee, M. Baghaban Eslaminejad, F. Mashhadiabbas, N. Tongas, M. Rasoulboroujeni, A. Yadegari, K. Ede, M. Tahriri, L. Tayebi, Influence of conductive PEDOT:PSS in a hard tissue scaffold: In vitro and in vivo study, 34(6) (2019) 436-441.
- [89] M. Yazdimamaghani, M. Razavi, M. Mozafari, D. Vashaei, H. Kotturi, L. Tayebi, Biomineralization and biocompatibility studies of bone conductive scaffolds containing poly(3,4-ethylenedioxythiophene):poly(4-styrene sulfonate) (PEDOT:PSS), *Journal of Materials Science: Materials in Medicine* 26(12) (2015) 274.